PHYSICAL REVIEW D
PARTICLES AND FIELDS

THIRD SERIES, VOLUME 35, NUMBER 6 15 MARCH 1987

Dynamics of false-vacuum bubbles

Steven K. Blau* and E. I. Guendelman†
Center for Theoretical Physics, Laboratory for Nuclear Science and Department of Physics, Massachusetts Institute of Technology, Cambridge, Massachusetts 02139

Alan H. Guth
Center for Theoretical Physics, Laboratory for Nuclear Science and Department of Physics, Massachusetts Institute of Technology, Cambridge, Massachusetts 02139
and Harvard-Smithsonian Center for Astrophysics, 60 Garden Street, Cambridge, Massachusetts 02138
(Received 3 November 1986)

The possibility of localized inflation is investigated by calculating the dynamics of a spherically symmetric region of false vacuum which is separated by a domain wall from an infinite region of true vacuum. For a range of initial conditions, the false-vacuum region will undergo inflation. An observer in the exterior true-vacuum region will describe the system as a black hole, while an observer in the interior will describe a closed universe which completely disconnects from the original spacetime. We suggest that this mechanism is likely to lead to an instability of Minkowski space: a region of space might undergo a quantum fluctuation into the false-vacuum state, evolving into an isolated closed universe; the black hole which remains in the original space would disappear by quantum evaporation. The formation of these isolated closed universes may also be relevant to the question of information loss in black-hole formation.

I. INTRODUCTION

An intriguing feature of the inflationary universe model[1–4] is the wide range of initial conditions which the model allows. One can imagine an initial spacetime manifold which is not at all homogeneous. The spacetime could be hot in some regions, cold in other regions, expanding in some regions, contracting in other regions, etc. One could argue that the regions which were both hot and expanding would cool down to the temperature of the inflationary phase transition. For an appropriate underlying particle theory, these regions would then undergo extreme supercooling, approaching the false-vacuum state. The unusual properties of the energy-momentum tensor for this state would then lead to the phenomenon of inflation, causing these regions to expand by many orders of magnitude to become much larger than the observed universe. We would then be living today deep inside one of these inflated regions. We could not be living in one of the regions that did not inflate, because those regions would have remained microscopic in size and would have no chance of producing life.

While the description given above seems plausible, the mathematical details have never been worked out. Most calculations for inflationary models have been carried out under the simplifying assumption of homogeneity, even though one assumes that initial homogeneity is not a necessary condition. There have also been calculations[5–10] which have used perturbation theory to study the mass density inhomogeneities caused by quantum effects, but these calculations rely on a homogeneous zero-order approximation. Thus, the consequences of large inhomogeneities in the initial conditions need to be elucidated.

The mathematics of inhomogeneous spacetimes can be very complex, so we will content ourselves to study only the simplest possible example. We will study the dynamics of a spherically [O(3)] symmetric universe that consists of a finite region of false vacuum separated by a domain wall from an infinite region of true vacuum. Although this system is highly simplified, it nonetheless raises two significant paradoxes.

The first paradox concerns the behavior of the volume of the false-vacuum region. If this region is sufficiently large, then an observer who makes measurements deep within the region would unambiguously expect to see inflation. However, an observer who makes measurements of the domain wall would have a different point of view. He would note that the false-vacuum region has negative pressure and is surrounded by the zero-pressure true vacu-

um. The pressure forces are therefore inward, reflecting the inherent instability of the false vacuum. Our assumption of spherical symmetry implies that the metric in the true-vacuum region has the usual Schwarzschild form, so gravitational effects are not expected to cause the false-vacuum region to expand into the true-vacuum region. Thus, the second observer does not expect to see inflation.

In fact, these two points of view are not contradictory. The key to reconciling them is an understanding of the non-Euclidean geometry of the spacetime manifold. We will discover that inflation does take place, for a sufficiently large region of false vacuum, but that the inflating false-vacuum region does not move out into the true-vacuum region.

The second paradox, first discussed by Sato, Kodama, Sasaki, and Maeda,[11] is concerned with the time evolution of the domain-wall radius of curvature. Suppose that this quantity is measured simultaneously by two observers, one of which is just inside the false-vacuum region, and the second of which is just on the other side of the domain wall. (Since the two observers can be arbitrarily close to each other, there is no difficulty in defining simultaneity.) Naively, we would expect the observer on the false-vacuum side to see the radius of curvature increase with the inflation of the false-vacuum region. On the other hand, we would expect that the observer on the true-vacuum side would not see an increase in the radius of curvature, since we have already concluded that the false-vacuum bubble does not expand into the true-vacuum region. General relativity guarantees, however, that the manifold be continuous, and it follows that the two observers must measure the same radius of curvature. Again, an understanding of the non-Euclidean geometry is the key to resolving this paradox. In particular, the resolution will hinge on the fact that the standard Schwarzschild coordinates fail to cover the entire manifold.

Although the problem which we solve is very idealized, we believe that it contains the essential physics of more complicated inhomogeneous spacetimes. The paradoxes discussed above will exist whenever an inflating region is surrounded by a noninflating region, and the qualitative behavior of the system will be determined by the manner in which these paradoxes are resolved.

In order to make the calculation tractable in closed form, we will make one further assumption in addition to that of spherical symmetry. The domain wall which separates the false-vacuum region from the true-vacuum region is in reality a dynamical object which can be described properly only by specifying the scalar field as a function of position. We will work, however, in the "thin-wall" approximation which assumes that the thickness of the wall is small compared to all other length scales in the problem and that the scalar field configuration has dynamically relaxed to its equilibrium form. Thus, the energy-momentum tensor for the wall is determined completely once the position of the wall is known.

The dynamics of the universe is completely specified once we have solved the Einstein equations in the true- and false-vacuum regions and once we have determined the evolution of the domain wall. The solution in the true-vacuum region is guaranteed by Birkhoff's theorem to be a Schwarzschild metric, with the parameter M signifying the mass of the system as detected from asymptotically large distances. In the false-vacuum region, once the energy density is specified, there is similarly a one-parameter class of spherically symmetric solutions. However, since the false-vacuum region comprises the interior of our configuration, we will consider only solutions that are regular at $r=0$. (Note that for spherically symmetric configurations $r=0$ can be defined in a coordinate-invariant way as the locus of points which are invariant under rotations.) It is easily shown that this additional requirement singles out the de Sitter space solution. The dynamics of the domain wall is specified by the requirements that the Einstein equations hold at the wall and that the tangential components of the metric remain continuous as the wall is crossed.

The behavior of regions of false vacuum that are surrounded by true vacuum was first studied by Sato *et al.*,[11,12] who were working in the context of the original inflationary universe model. They considered the case in which an infinite number of true-vacuum bubbles are nucleated on the surface of a sphere, leaving a trapped region of false vacuum in the interior.[13] The mathematical problem which they solved is then identical to the one that we consider, except that they avoided the complicated dynamics by working in the approximation that the domain wall moves at the speed of light. This approximation is valid, for plausible physical parameters, except for a brief period during which the domain wall changes direction. In one of their papers[14] they included the possibility that the true-vacuum region could have a nonzero energy density.

In this paper we use a mathematical formalism which was developed primarily by Israel,[15] and which has been used by several previous authors. The collapse of domain walls separating two regions of true vacuum has been studied by Ipser and Sikivie.[16] They however limited their study to the case in which the domain wall lies outside the Schwarzschild horizon, and therefore bypassed the unusual features of the spacetime geometry. The dynamics of domain walls separating regions of true or false vacua with arbitrary non-negative energy densities has been investigated by Berezin, Kuzmin, and Tkachev[17,18] and by Aurilia, Denardo, Legovini, and Spallucci.[19]

We will attempt to give a clearer and more detailed description of the spacetime geometry than the previous authors, and we will also present a more systematic catalog of the possible solutions. Our results disagree in some respects with those of Berezin, Kuzmin, and Tkachev, and Aurilia, Denavdo, Legovini, and Spalluci, and these disagreements will be pointed out in Secs. IV and V and also in Appendixes C and D.

In the next section we will review the Gauss-Codazzi formalism, in which four-dimensional spacetime is parametrized by a one-parameter family of three-dimensional hypersurfaces; four-dimensional geometric quantities are then expressed in terms of three-dimensional geometric quantities related to these hypersurfaces. The Einstein equations in this $(3+1)$-

dimensional language yield junction conditions which determine the dynamics of the domain wall, given the wall's energy-momentum tensor. In Sec. III we derive the form of the energy-momentum tensor for a domain wall, and in Sec. IV this result is combined with the solutions to the Einstein equations in the true- and false-vacuum regions to determine the equations of motion for the wall. In Sec. V we discuss the solutions of these equations of motion. We end with a summary which discusses some of the implications of these results.

II. JUNCTION CONDITIONS

In this section we will use the Einstein field equations to derive the equations which govern the evolution of the domain wall. These equations are called junction conditions because they describe the discontinuity, or junction, between the true- and false-vacuum regions.

The four-dimensional Einstein equations are

$$R_{\mu\nu}-\tfrac{1}{2}g_{\mu\nu}R=8\pi G T_{\mu\nu} , \tag{2.1}$$

where the metric has one negative eigenvalue, $R_{\mu\nu}$ is the Ricci tensor, R is the Ricci scalar, and $T_{\mu\nu}$ is the matter energy-momentum tensor.[20]

For the system under consideration,

$$T_{\mu\nu}=\begin{cases}-\rho_0 g_{\mu\nu} & \text{in false-vacuum region} ,\\ 0 & \text{in true-vacuum region} ,\end{cases} \tag{2.2}$$

and (in the thin-wall approximation) $T_{\mu\nu}$ has a δ-function singularity on the domain wall. Here ρ_0 denotes the energy density of the false vacuum.

To describe the behavior of the domain wall, it is simplest to introduce a Gaussian normal coordinate system in the neighborhood of the wall. Denoting the $(2+1)$-dimensional spacetime hypersurface swept out by the domain wall as Σ, we begin by introducing a coordinate system on Σ. For definiteness, two of the coordinates can be taken to be the angular variables θ and ϕ which are always well defined, up to an overall rotation, for a spherically symmetric configuration. For the third coordinate, one can use the proper-time variable τ that would be measured by an observer moving along with the domain wall. Next, consider all the geodesics which are orthogonal to Σ. Choose a neighborhood N about Σ so that any point $p\in N$ lies on one, and only one, geodesic. The first three coordinates of p are then determined by the coordinates of the intersection of this geodesic with Σ. Since Σ is orientable, we may regard one side of Σ as being the "positive direction." For definiteness, we take the true-vacuum side as positive. The fourth coordinate η of any $p\in N$ is then taken as the proper distance in the positive direction from Σ to p along the geodesic passing through p. Thus, the full set of coordinates is given by $x^\mu\equiv(x^i,\eta)$, where $x^i\equiv(\tau,\theta,\phi)$, and i runs from 1 to 3.

In these coordinates the metric obeys the following simplifying conditions:

$$g^{\eta\eta}=g_{\eta\eta}=1, \quad g^{\eta i}=g_{\eta i}=0 . \tag{2.3}$$

Furthermore, one can define a unit vector field $\xi^\mu(x)$ which is normal to each of the $\eta=$const hypersurfaces and pointing from the de Sitter to the Schwarzschild spacetime. In the Gaussian normal coordinates, this vector field is given by

$$\xi^\mu(x)=\xi_\mu(x)=(0,0,0,1) . \tag{2.4}$$

The extrinsic curvature corresponding to each $\eta=$const hypersurface is a three-dimensional tensor whose components are defined by

$$K_{ij}=\xi_{i;j} . \tag{2.5}$$

Here the semicolon represents the four-dimensional covariant derivative with respect to whatever index follows it, but the indices are restricted to the range of 1–3. In the Gaussian normal coordinates, the extrinsic curvature acquires the simple form

$$K_{ij}=-\Gamma^\eta_{ij}=\tfrac{1}{2}\partial_\eta g_{ij} . \tag{2.6}$$

One can easily see that K_{ij} is a symmetric tensor.

The Gauss-Codazzi formalism[15,21] is a method of viewing four-dimensional spacetime as being sliced up into three-dimensional hypersurfaces. At any point, the four-dimensional tensors $R_{\mu\nu\sigma\tau}$, $R_{\mu\nu}$, and R may be expressed in terms of the corresponding three-dimensional tensors and the extrinsic curvature of the hypersurface passing through the given point. The Gauss-Codazzi formalism does not require the use of Gaussian normal coordinates, but the formalism can be derived and expressed very simply with the use of these coordinates. One begins by noting that the only nonzero components of the affine connection are given by

$$\Gamma^k_{ij}={}^{(3)}\Gamma^k_{ij}, \quad \Gamma^\eta_{ij}=-K_{ij}, \quad \Gamma^i_{\eta j}=K^i{}_j , \tag{2.7}$$

where the superscript (3) denotes three-dimensional geometric quantities. It can then be shown that the Einstein equations become

$$G^\eta{}_\eta\equiv-\tfrac{1}{2}{}^{(3)}R+\tfrac{1}{2}[(\mathrm{Tr}K)^2-\mathrm{Tr}(K^2)] =8\pi G T^\eta{}_\eta , \tag{2.8a}$$

$$G^\eta{}_i\equiv K_i{}^m{}_{|m}-(\mathrm{Tr}K)_{|i}=8\pi G T^\eta{}_i , \tag{2.8b}$$

$$G^i{}_j\equiv{}^{(3)}G^i{}_j-(K^i{}_j-\delta^i{}_j\mathrm{Tr}K)_{,\eta}-(\mathrm{Tr}K)K^i{}_j +\tfrac{1}{2}\delta^i{}_j[\mathrm{Tr}K^2+(\mathrm{Tr}K)^2]=8\pi G T^i{}_j , \tag{2.8c}$$

where a comma denotes an ordinary derivative and a subscript vertical bar denotes the three-dimensional covariant derivative.

The energy-momentum tensor $T^{\mu\nu}$ is expected to have a δ-function singularity at the domain wall, so one can define the surface stress-energy tensor $S^{\mu\nu}$ by writing

$$T^{\mu\nu}(x)=S^{\mu\nu}(x^i)\delta(\eta)+(\text{regular terms}) . \tag{2.9}$$

In the next section we will discuss the form of $S^{\mu\nu}$ and will show that energy-momentum conservation implies $S^{\eta\eta}=S^{\eta i}=0$.

When the energy-momentum tensor of Eq. (2.9) is inserted into the field equations (2.8), one sees that (2.8a) and (2.8b) are satisfied automatically provided that they are satisfied for $\eta\neq0$ and provided that g_{ij} is continuous at $\eta=0$ (so that K_{ij} does not acquire a δ-function singu-

larity). Equation (2.8c) then leads to the junction condition

$$\gamma^i{}_j-\delta^i{}_j\mathrm{Tr}\gamma=-8\pi G S^i{}_j\ , \tag{2.10}$$

where

$$\gamma_{ij}=\lim_{\epsilon\to 0}[K_{ij}(\eta=+\epsilon)-K_{ij}(\eta=-\epsilon)]\ . \tag{2.11}$$

By taking the trace of Eq. (2.10) we obtain $\mathrm{Tr}\gamma=4\pi G\,\mathrm{Tr}S$, which can be substituted back into Eq. (2.10) to give

$$\gamma^i{}_j=-8\pi G(S^i{}_j-\tfrac{1}{2}\delta^i{}_j\mathrm{Tr}S)\ . \tag{2.12}$$

A discussion of the meaning of this equation will be postponed until the properties of $S^{\mu\nu}$ are analyzed in the next section.

III. SURFACE STRESS ENERGY OF A DOMAIN WALL

In this section we will use symmetry arguments and energy-momentum conservation to determine the form of the surface stress energy defined by Eq. (2.9). For convenience we will use the Gaussian normal coordinate system described in the previous section.

The thin-wall approximation assumes that the thickness of the domain wall is much less than any other length scale in the problem. On scales much larger than the thickness, the energy-momentum tensor of the wall can be accurately approximated by an expression proportional to a δ function on the wall, $\delta(\eta)$, as in Eq. (2.9). Implicit in this description is the assumption that the domain wall has settled into an equilibrium configuration—otherwise it would radiate energy as it approached its equilibrium form, and the energy-momentum distribution would not remain confined to a thin wall.

Using Eq. (2.7), one can easily write down the equations for energy-momentum conservation in Gaussian normal coordinates:

$$T^{i\nu}{}_{;\nu}=T^{ij}{}_{|j}+T^{i\eta}{}_{,\eta}+2K^i{}_jT^{j\eta}+(\mathrm{Tr}K)T^{i\eta}=0\ , \tag{3.1a}$$

$$T^{\eta\nu}{}_{;\nu}=T^{\eta i}{}_{|i}+T^{\eta\eta}{}_{,\eta}-K_{ij}T^{ij}+(\mathrm{Tr}K)T^{\eta\eta}=0\ . \tag{3.1b}$$

For the case of interest, $T^{\mu\nu}$ can be written as

$$T^{\mu\nu}(x)=S^{\mu\nu}(x^i)\delta(\eta)-\rho_0\theta(-\eta)g^{\mu\nu}\ . \tag{3.2}$$

Combining (3.2) with (3.1a), one finds

$$T^{i\nu}{}_{;\nu}=[S^{ij}{}_{|j}+2K^i{}_jS^{j\eta}+(\mathrm{Tr}K)S^{i\eta}]\delta(\eta)+S^{i\eta}\delta'(\eta)=0\ , \tag{3.3}$$

where the prime denotes differentiation with respect to η. Note that Eq. (3.3) appears to contain an ambiguity, since K_{ij} must be evaluated at $\eta=0$ where it is discontinuous. The problem arises because we are computing the gravitational force on a sheet of mass, a situation which is completely analogous to the elementary problem of evaluating the electrostatic force on a sheet of charge. However, by setting the coefficient of $\delta'(\eta)$ in Eq. (3.3) to zero, one learns that

$$S^{i\eta}=0\ , \tag{3.4}$$

and the ambiguity disappears. The vanishing of the term in $\delta(\eta)$ then implies that

$$S^{ij}{}_{|j}=0\ . \tag{3.5}$$

From (3.1b) one finds

$$T^{\eta\nu}{}_{;\nu}=[\rho_0-\bar{K}_{ij}S^{ij}+(\mathrm{Tr}K)S^{\eta\eta}]\delta(\eta)+S^{\eta\eta}\delta'(\eta)=0\ , \tag{3.6}$$

where

$$\bar{K}_{ij}=\lim_{\epsilon\to 0}\tfrac{1}{2}[K_{ij}(\eta=+\epsilon)+K_{ij}(\eta=-\epsilon)]\ . \tag{3.7}$$

In this case the ambiguity does not disappear, but it will be shown in Appendix A that it can be resolved exactly as in the electrostatic example, with the result which is shown above. One can then deduce that

$$S^{\eta\eta}=0 \tag{3.8}$$

and that

$$\bar{K}_{ij}S^{ij}=\rho_0\ . \tag{3.9}$$

Combining the orthogonality conditions (3.4) and (3.8) with rotational invariance, one concludes that $S^{\mu\nu}$ can be written as

$$S^{\mu\nu}=\sigma(\tau)U^\mu U^\nu-\zeta(\tau)(h^{\mu\nu}+U^\mu U^\nu)\ , \tag{3.10}$$

where

$$h^{\mu\nu}=g^{\mu\nu}-\xi^\mu\xi^\nu \tag{3.11}$$

is the metric projected into the hypersurface of the wall, and

$$U^\mu=(1,0,0,0) \tag{3.12}$$

is the four-velocity of the domain wall. Here σ is the surface energy density of the domain wall, and ζ is the surface tension. Rotational invariance also implies that the metric on the domain wall can be written as

$$ds^2=-d\tau^2+r^2(\tau)d\Omega^2\ , \tag{3.13}$$

where $d\Omega^2\equiv d\theta^2+\sin^2\theta\,d\phi^2$. Equation (3.5) then reduces to

$$\dot{\sigma}=-2(\sigma-\zeta)\frac{\dot{r}}{r}\ , \tag{3.14}$$

where the overdot denotes a derivative with respect to τ. By introducing the area $A=4\pi r^2$ of the sphere, the above equation can be rewritten as

$$\frac{d}{d\tau}(A\sigma)=\zeta\frac{dA}{d\tau}\ , \tag{3.15}$$

a formula which is easily identified as the conservation of energy.

The values of σ and ζ are further restricted by the underlying dynamics of the scalar field which comprises the domain wall, which has an energy-momentum tensor

$$T_{\mu\nu}=\partial_\mu\phi\partial_\nu\phi-g_{\mu\nu}[\tfrac{1}{2}\partial_\sigma\phi\partial_\tau\phi g^{\sigma\tau}+V(\phi)]\ . \tag{3.16}$$

Note that the thin-wall approximation assumes that any

variation of ϕ along the wall occurs only on length scales much larger than the wall thickness, and so $\partial_\mu\phi \propto \xi_\mu$ to a high degree of accuracy. Thus $T_{\mu\nu}$ can only have terms proportional to $\xi_\mu\xi_\nu$ or to $g_{\mu\nu}$, and it follows that $\zeta=\sigma$. It then follows from (3.14) that $\dot{\sigma}=0$, and so finally

$$S^{\mu\nu}(x^i)=-\sigma h^{\mu\nu}(x^i,\eta=0)\ . \tag{3.17}$$

Before closing this section we would like to discuss the intuitive meaning of Eqs. (2.12) and (3.9). Note that

$$K_{\tau\tau}=\xi_{\tau;\tau}=U^\mu U^\nu\xi_{\mu;\nu}=-\xi_\mu U^\nu U^\mu{}_{;\nu}=-\xi_\mu\frac{DU^\mu}{D\tau}\ , \tag{3.18}$$

where $DU^\mu/D\tau\equiv dU^\mu/d\tau+\Gamma^\mu_{\lambda\sigma}U^\lambda U^\sigma$ is the covariant acceleration of the wall. Thus $K_{\tau\tau}$ is the component of the covariant acceleration in the normal direction, which is in fact the only nonzero component. The discontinuity of $K_{\tau\tau}$ [proportional to $(\sigma-2\zeta)$] implied by (2.12) therefore represents a discontinuity in the acceleration of locally inertial frames. One has also

$$K_{\theta\theta}=\frac{K_{\phi\phi}}{\sin^2\theta}=\tfrac{1}{2}\partial_\eta r^2\ , \tag{3.19}$$

so the discontinuity in the angular components of the extrinsic curvature (proportional to σ) measures the discontinuity of geometric distortion.

Finally, Eq. (3.9) can be written as

$$\sigma\left\langle\xi_\mu\frac{DU^\mu}{D\tau}\right\rangle=-\frac{\zeta}{r^2}\langle\partial_\eta r^2\rangle-\rho_0\ , \tag{3.20}$$

where the angular brackets mean that the indicated quantity is to be averaged over the values it has on either side of the discontinuity at $\eta=0$. The above equation is easily identified as the equation of motion for a spherical membrane with surface tension ζ and a constant pressure difference ρ_0 pointing inward.

IV. EQUATIONS OF MOTION FOR A DOMAIN WALL

In this section we will discuss the solutions to the Einstein equations in the true- and false-vacuum regions, and we will then combine these results with those of the previous two sections to obtain the equations of motion for the domain wall.

The most general O(3)-symmetric solution to the Einstein equations for a region of spacetime with vanishing cosmological constant and matter energy-momentum tensor is given by Birkhoff's theorem as

$$-d\tau^2=ds^2=-\left[1-\frac{2GM}{R}\right]dT^2+\left[1-\frac{2GM}{R}\right]^{-1}dR^2 +R^2d\Omega^2\ , \tag{4.1}$$

where M is an as yet undetermined parameter. Equation (4.1) presents the Schwarzschild line element, which describes the true-vacuum side of the domain wall. We will let the lower-case letters r and t denote the values of the corresponding Schwarzschild coordinates at the domain wall, and we will think of these quantities as functions of the proper time τ measured along the domain-wall trajectory. The value of $r(\tau)$ has a meaning that can be described in a coordinate-invariant way: it is the proper length of an arc on the domain wall subtending an angle $d\alpha$, divided by the angle $d\alpha$. One therefore calls $r(\tau)$ the proper circumferential radius of the domain wall.

The standard Schwarzschild metric displayed in Eq. (4.1) has a singularity at the horizon, $R=2GM$, but this is an unphysical singularity caused by a poor choice of coordinates. In the problem under consideration much of the interesting physics happens inside the horizon, so it is important that we use a coordinate system which behaves smoothly as the horizon is crossed. For this reason we will work with the Kruskal-Szekeres[22] coordinate system (V,U,θ,ϕ), which for $R>2GM$ is related to the usual coordinates by

$$\begin{aligned}U&=\left[\frac{R}{2GM}-1\right]^{1/2}\exp\left[\frac{R}{4GM}\right]\cosh\left[\frac{T}{4GM}\right]\ ,\\ V&=\left[\frac{R}{2GM}-1\right]^{1/2}\exp\left[\frac{R}{4GM}\right]\sinh\left[\frac{T}{4GM}\right]\ ,\end{aligned} \tag{4.2a}$$

while the coordinates θ and ϕ retain their original meanings. Equations (4.2a) define what we will call region I of the Schwarzschild space. For $R<2GM$ the Kruskal-Szekeres coordinates are related by

$$\begin{aligned}U&=\left[1-\frac{R}{2GM}\right]^{1/2}\exp\left[\frac{R}{4GM}\right]\sinh\left[\frac{T}{4GM}\right]\ ,\\ V&=\left[1-\frac{R}{2GM}\right]^{1/2}\exp\left[\frac{R}{4GM}\right]\cosh\left[\frac{T}{4GM}\right]\ ,\end{aligned} \tag{4.2b}$$

which define region II. These relationships are illustrated in Fig. 1. The values of the coordinates U and V at the domain wall will be called u and v, respectively.

The coordinate singularity has now been eliminated, and the line element (4.1) becomes

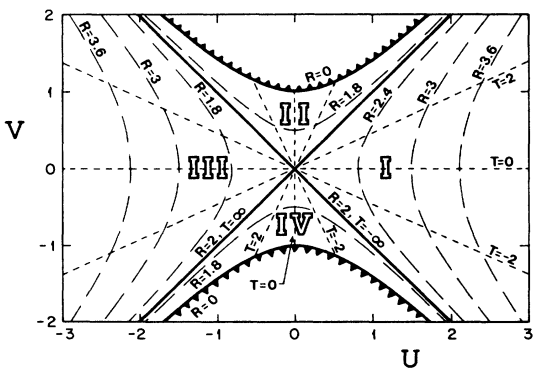

FIG. 1. A diagram of the Kruskal-Szekeres coordinate system. The four regions are labeled I, II, III, and IV, and lines of constant R and T are shown. The lines are labeled in units of GM.

$$-d\tau^2=ds^2=\frac{32(GM)^3}{R}\exp\left[\frac{-R}{2GM}\right](-dV^2+dU^2)$$
$$+R^2d\Omega^2\,, \tag{4.3}$$

where R is a function of U and V given by

$$\left[\frac{R}{2GM}-1\right]\exp\left[\frac{R}{2GM}\right]=U^2-V^2\,. \tag{4.4}$$

The metric is defined only for the region $U^2-V^2>-1$, and the boundary at $U^2-V^2=-1$ corresponds to the physical singularity at $R=0$. Note that the line element (4.3) implies that lightlike trajectories lie at 45° relative to the U and V axes.

The Schwarzschild coordinate system has thus been mapped entirely into the half-space $U+V>0$. The boundary at $U+V=0$ can be reached by (past directed) timelike trajectories in a finite proper time; therefore it must be viewed as a physical boundary of the manifold covered by the Schwarzschild coordinates. Since physical boundaries are generally considered unacceptable, it is standard practice to extend the manifold to include all values of U and V satisfying $U^2-V^2>-1$. We will henceforth refer to this extended manifold as Schwarzschild space. It is often useful to introduce Schwarzschild coordinates R and T in the two new quadrants, with the relations

$$U=-\left[\frac{R}{2GM}-1\right]^{1/2}\exp\left[\frac{R}{4GM}\right]\cosh\left[\frac{T}{4GM}\right]\,,$$
$$V=-\left[\frac{R}{2GM}-1\right]^{1/2}\exp\left[\frac{R}{4GM}\right]\sinh\left[\frac{T}{4GM}\right]\,, \tag{4.5a}$$

in the region $U<0, |V|<|U|$ (region III), and

$$U=-\left[1-\frac{R}{2GM}\right]^{1/2}\exp\left[\frac{R}{4GM}\right]\sinh\left[\frac{T}{4GM}\right]\,,$$
$$V=-\left[1-\frac{R}{2GM}\right]^{1/2}\exp\left[\frac{R}{4GM}\right]\cosh\left[\frac{T}{4GM}\right]\,, \tag{4.5b}$$

in the region $V<0, |U|<|V|$ (region IV). The line element maintains the usual form (4.1) when expressed in terms of R and T. These new regions are also shown in Fig. 1.

The full manifold for our problem contains a region of Schwarzschild space, a region of de Sitter space, and a boundary which separates them. Since the Schwarzschild spacetime has the symmetry $U\rightarrow -U$, we can always choose a coordinate system so that the Schwarzschild region lies to the right of the boundary in th U-V plane [i.e., so that the Schwarzschild region can be described by $U>u(\tau)$]. Since the normal vector field $\xi^\mu(x)$ is defined to point from the de Sitter to the Schwarzschild spacetime, it follows that $\xi^\mu(x)$ points to increasing values of the coordinate U.

There are a number of different coordinate systems which are frequently used to describe de Sitter space, and the choice is determined entirely by convenience. The static coordinate system, with its line element

$$-d\tau^2=ds^2=-(1-\chi^2R^2)dT^2+(1-\chi^2R^2)^{-1}dR^2$$
$$+R^2d\Omega^2\,, \tag{4.6}$$

provides a close parallel to the static Schwarzschild metric of Eq. (4.1). (We are using the same symbols for the coordinates, trusting that the context will make it clear which spacetime is being described.) Like the Schwarzschild coordinate system, the de Sitter static coordinate system suffers from three defects: lightlike lines are difficult to identify, the coordinate system does not cover the entire manifold, and there appears to be a singularity at the horizon. These defects can be remedied in a number of ways, but we choose to maintain a close parallel with the Kruskal-Szekeres construction by using the Gibbons-Hawking coordinate system[23] for de Sitter space. The relation between the Gibbons-Hawking coordinates and several better-known de Sitter-space coordinate systems is given in Appendix B. The Gibbons-Hawking coordinates (U,V,θ,ϕ) are related to the static coordinates for $R<\chi^{-1}$ by

$$U=\left[\frac{1-\chi R}{1+\chi R}\right]^{1/2}\cosh(\chi T)\,,$$
$$V=\left[\frac{1-\chi R}{1+\chi R}\right]^{1/2}\sinh(\chi T)\,. \tag{4.7}$$

The static coordinate system thus covers one quadrant of the U-V plane, which we call region I. These relationships are illustrated in Fig. 2. The new line element is given by

$$-d\tau^2=ds^2=\chi^{-2}(1+\chi R)^2(-dV^2+dU^2)$$
$$+R^2d\Omega^2\,, \tag{4.8}$$

where R is a function of U and V given by

$$\frac{1-\chi R}{1+\chi R}=U^2-V^2\,. \tag{4.9}$$

It is straightforward to extend the metric (4.8) over the

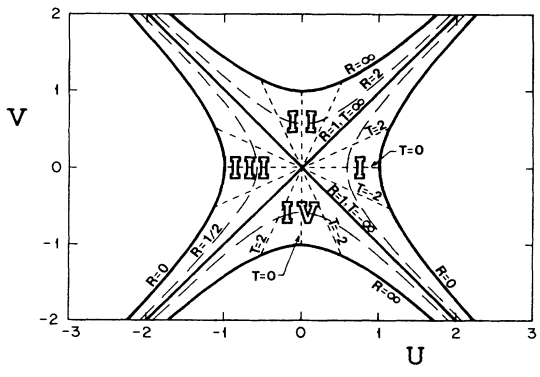

FIG. 2. A diagram of the Gibbons-Hawking coordinate system of de Sitter space, which is a close analog of the Kruskal-Szekeres coordinate system of Schwarzschild space. The four regions are labeled I, II, III, and IV, and lines of constant R and T are shown. The labeling is in units of χ^{-1}.

entire U-V plane, subject to the restriction $|U^2-V^2|<1$. The coordinate system then covers the entire de Sitter manifold.

It is useful to introduce coordinates R and T into the other three quadrants, with the relation

$$U=\left[\frac{\chi R-1}{\chi R+1}\right]^{1/2}\sinh(\chi T)\ ,$$
$$V=\left[\frac{\chi R-1}{\chi R+1}\right]^{1/2}\cosh(\chi T)\ , \tag{4.10a}$$

in the region $V>0, |U|<V$ (region II),

$$U=-\left[\frac{1-\chi R}{1+\chi R}\right]^{1/2}\cosh(\chi T)\ ,$$
$$V=-\left[\frac{1-\chi R}{1+\chi R}\right]^{1/2}\sinh(\chi T)\ , \tag{4.10b}$$

in the region $U<0, |V|<|U|$ (region III), and

$$U=-\left[\frac{\chi R-1}{\chi R+1}\right]^{1/2}\sinh(\chi T)\ ,$$
$$V=-\left[\frac{\chi R-1}{\chi R+1}\right]^{1/2}\cosh(\chi T)\ , \tag{4.10c}$$

in the region $V<0, |U|<|V|$ (region IV). These new regions are also shown in Fig. 2.

Like the Schwarzschild spacetime, the de Sitter spacetime has the symmetry $U\rightarrow -U$. This time we will use the symmetry to choose our coordinates so that the de Sitter region lies to the left of the boundary in the U-V plane [i.e., so that the de Sitter region is described by $U<u(\tau)$]. The normal vector $\xi^\mu(x)$ will again point to increasing values of U.

Our goal is to use the junction condition (2.12) to derive a dynamical equation for the proper circumferential radius of the domain wall. The Schwarzschild and de Sitter line elements along with the behavior of $r(\tau)$ specify completely the system parametrized by the mass M.

By combining (2.12) with the expression (3.17) for the surface stress-energy $S^{\mu\nu}$, one finds

$$\gamma^i{}_j\equiv K^i{}_j(\text{Schwarzschild})-K^i{}_j(\text{de Sitter})$$
$$=-4\pi\sigma G\delta^i{}_j\ . \tag{4.11}$$

It is now straightforward to calculate the components of the extrinsic curvature as seen by Schwarzschild and de Sitter observers, and to then use Eq. (4.11) to ascertain the dynamics of the bubble wall. The calculation is facilitated by using Gaussian normal coordinates, so that the extrinsic curvature is given by Eq. (2.6).

Spherical symmetry guarantees that the off-diagonal components of the extrinsic curvature vanish, and that the angular components are related by $K_{\phi\phi}=\sin^2\theta K_{\theta\theta}$. Thus the dynamics of the domain wall are completely specified by the $\theta\theta$ and $\tau\tau$ components of Eq. (4.11).

We may evaluate the $\theta\theta$ component of Eq. (4.11) by starting with Eq. (3.19). From

$$K_{\theta\theta}=\tfrac{1}{2}\partial_\eta r^2=\tfrac{1}{2}\xi^\mu\partial_\mu r^2\ , \tag{4.12}$$

we can see that the key step is to evaluate the normal vector $\xi^\mu(x)$ on the domain wall.

We begin by calculating the normal vector as seen by a Schwarzschild observer. Because the domain wall is spherically symmetric, the four-velocity of any point on the wall assumes the form

$$U^\mu_{\rm KS}=(\dot v,\dot u,0,0) \tag{4.13}$$

in Kruskal-Szekeres coordinates, with an overdot signifying differentiation with respect to proper time, and

$$U^\mu_S=(\dot t,\dot r,0,0) \tag{4.14}$$

in the standard Schwarzschild coordinates. We choose the flow of proper time so that future directed world lines satisfy $\dot V>0$.

Since the unit normal ξ^μ is orthogonal to U^μ and points to increasing values of U, it follows that

$$\xi^\mu_{\rm KS}=(\dot u,\dot v,0,0) \tag{4.15}$$

in Kruskal-Szekeres coordinates. Transforming to the standard Schwarzschild coordinates one finds

$$\xi^\mu_S=(A_S{}^{-1}\dot r,\beta_S,0,0)\ , \tag{4.16}$$

where

$$A_S=1-\frac{2GM}{r} \tag{4.17}$$

and

$$\beta_S=A_S\dot t_{(S)} \tag{4.18a}$$
$$=\frac{8(GM)^2}{r}e^{-r/2GM}(u\dot v-v\dot u)\ . \tag{4.18b}$$

The subscript (S) appears in Eq. (4.18a) to emphasize that t in this equation represents the Schwarzschild time variable. One can relate $\dot t_{(S)}$ to $\dot r$ by using the normalization of the velocity four-vector U^μ_S, with the result that

$$\beta_S=\pm(A_S+\dot r^2)^{1/2}\ . \tag{4.18c}$$

By applying Eq. (4.12) in the Schwarzschild system, one has immediately that

$$K_{\theta\theta}(\text{Schwarzschild})=r\beta_S\ . \tag{4.19}$$

The form (4.18c) for β_S will prove to be the most useful, since it is expressed in terms of the quantity $\dot r$, which has a coordinate invariant interpretation. The sign ambiguity is resolved by using the form (4.18b), which leads to a simple geometric prescription: β_S is positive if the polar angle $\arctan(v/u)$ increases as one moves along the domain-wall trajectory, and it is negative if the angle decreases.

One now repeats these steps for the normal vector as seen by a de Sitter observer. One finds

$$U^\mu_{\rm GH}=(\dot v,\dot u,0,0) \tag{4.20}$$

in the Gibbons-Hawking coordinates, and that

$$U^\mu_{\rm stat}=(\dot t,\dot r,0,0) \tag{4.21}$$

in the de Sitter static coordinates. The normal vector is then given by

$$\xi^{\mu}_{\rm GH}=(\dot{u},\dot{v},0,0)\ , \tag{4.22}$$

which can then be transformed to give

$$\xi^{\mu}_{\rm stat}=(A_D{}^{-1}\dot{r},\beta_D,0,0)\ , \tag{4.23}$$

where

$$A_D=1-\chi^2r^2 \tag{4.24}$$

and

$$\beta_D=A_D\dot{t}_{(D)} \tag{4.25a}$$

$$=-\chi^{-1}(1+\chi r)^2(u\dot{v}-v\dot{u})\ , \tag{4.25b}$$

where the subscript (D) has been added to emphasize that here t refers to the de Sitter static time coordinate.

By normalizing the velocity four-vector, one finds

$$\beta_D=\pm(A_D+\dot{r}^2)^{1/2}\ . \tag{4.25c}$$

Finally,

$$K_{\theta\theta}(\text{de Sitter})=r\beta_D\ . \tag{4.26}$$

The most useful form for β_D will be (4.25c), with the sign ambiguity resolved by (4.25b). Again there is a simple geometric prescription for the sign, but it is the opposite of the Schwarzschild case; β_D is positive if the polar angle $\arctan(v/u)$ decreases as one moves along the domain-wall trajectory, and it is negative if the angle increases.

The $\theta\theta$ component of Eq. (4.11) may now be written

$$\beta_D-\beta_S=4\pi G\sigma r\ , \tag{4.27}$$

with β_D and β_S defined in Eqs. (4.25) and (4.18), respectively. In the next section we will use this equation to determine the properties of the solution to our problem. However, there are a few points which we would first like to discuss.

The $\tau\tau$ component of Eq. (4.11) is linearly independent from the angular components, so it is worthwhile to check its implication. With the help of Eq. (3.18) one calculates $K_{\tau\tau}$ to be

$$K_{\tau\tau}=\begin{cases}-\dfrac{1}{\beta_S}\left[\ddot{r}+\dfrac{GM}{r^2}\right] & \text{Schwarzschild case}\ ,\\ -\dfrac{1}{\beta_D}(\ddot{r}-\chi^2r) & \text{de Sitter case}\ .\end{cases} \tag{4.28}$$

One then finds that the $\tau\tau$ component of Eq. (4.11) is simply the proper-time derivative of Eq. (4.27). Indeed, it is not surprising that there should be a functional relationship between the time and angular components of (4.11); such a relationship is guaranteed by the fact that the Einstein equations imply conservation of $T_{\mu\nu}$, but the $T_{\mu\nu}$ used in this calculation is manifestly conserved.

An equation for $\ddot{r}$ can also be obtained by substituting the expressions for K_{ij} into (3.20), which was derived directly from the conservation of $T_{\mu\nu}$. One finds

$$\frac{1}{2}\left[\frac{1}{\beta_S}+\frac{1}{\beta_D}\right]\sigma\ddot{r}=-\frac{(\beta_D+\beta_S)\zeta}{r}-\frac{GM\sigma}{2\beta_Sr^2}+\frac{\sigma\chi^2r}{2\beta_D}-\rho_0\ , \tag{4.29}$$

and one can verify that this equation is equivalent to the $\tau\tau$ component of Eq. (4.11). In the nonrelativistic limit the terms on the right-hand side of (4.29) can be identified as the surface tension, the gravitational attraction, the de Sitter repulsion, and the pressure difference. Recall that in the case of interest $\zeta=\sigma$.

Equation (4.27) allows one to express the mass M of the bubble wall in terms of r and $\dot{r}$ as

$$M=\frac{\chi^2r^3}{2G}+4\pi\sigma r^2(1-\chi^2r^2+\dot{r}^2)^{1/2}\text{sgn}\beta_D$$

$$-8\pi^2G\sigma^2r^3\ . \tag{4.30}$$

It is instructive to consider the limiting case $\chi^2r^2,\dot{r}^2\ll1$, $\text{sgn}\beta_D=+1$. Then

$$M\approx\frac{\chi^2r^3}{2G}+4\pi\sigma r^2(1+\dot{r}^2)^{1/2}-2\pi\sigma\chi^2r^4$$

$$-8\pi^2G\sigma^2r^3\ . \tag{4.31}$$

We recognize the four terms of Eq. (4.31) in order as the volume energy of the bubble, the surface energy of the bubble, with lowest-order relativistic correction, the Newtonian surface-volume binding energy, and the Newtonian surface-surface binding energy. Curiously, there is no volume-volume interaction term.

Equation (4.30) agrees with Eq. (6) of Berezin, Kuzmin, and Tkachev,[17] except that these authors allow the true-vacuum energy density to be nonzero, and that they do not draw the connection between $\text{sgn}\beta_D$ and the rate of change of the polar angle in the de Sitter diagram. Aurilia, Denardo, Legovini, and Spallucci[19] have a similar equation, which appears as Eq. (18) of the first paper cited and as Eq. (4.5) of the second paper. Some of their signs, however, are in disagreement with ours.

V. SOLUTION OF THE EQUATIONS OF MOTION

We will now discuss the solutions of the equations of motion derived in the previous section.

The key equation is (4.27), where β_D and β_S are defined by Eqs. (4.25) and (4.18), respectively. We write Eq. (4.27) by bringing β_S to the right-hand side and then squaring, with the result

$$2GM=\chi_+{}^2r^3+2\kappa r^2\beta_S\ , \tag{5.1}$$

where

$$\kappa\equiv4\pi G\sigma \tag{5.2}$$

and

$$\chi_+{}^2\equiv\chi^2+\kappa^2\ . \tag{5.3}$$

We now introduce the dimensionless variables

$$z^3 \equiv \frac{\chi_+^2}{2GM} r^3 \tag{5.4}$$

and

$$\tau' \equiv \frac{\chi_+^2 \tau}{2\kappa} . \tag{5.5}$$

Equation (5.1) can then be rewritten as

$$1 = z^3 \pm z^2 \left[\left[\frac{dz}{d\tau'} \right]^2 - \frac{\gamma^2}{z} - E \right]^{1/2} , \tag{5.6}$$

where

$$E \equiv \frac{-4\kappa^2}{(2GM)^{2/3} \chi_+^{8/3}} \tag{5.7}$$

and

$$\gamma \equiv \frac{2\kappa}{\chi_+} . \tag{5.8}$$

Note that $0 \leq |\gamma| \leq 2$. From (5.6) one has

$$\left[\frac{dz}{d\tau'} \right]^2 + V(z) = E , \tag{5.9}$$

where

$$V(z) = -\left[\frac{1-z^3}{z^2} \right]^2 - \frac{\gamma^2}{z} . \tag{5.10}$$

The equation of motion of the domain wall is thus identical to that of a particle moving in one dimension under the influence of a potential.[24] A formal solution is then given by

$$\int^z \frac{dz'}{\sqrt{E - V(z')}} = \tau' . \tag{5.11}$$

While it is clear that any solution to Eq. (4.27) is also a solution to Eq. (5.9), a small discussion is required to justify the converse. In obtaining Eq. (5.1) from (4.27), we have squared both sides of an equation of the form $\beta_D = \cdots$. This operation can potentially introduce spurious solutions, but one can easily see that in this case it does not. The reason is that Eq. (4.27) provides a valid solution to our problem for either sign of the square-root function which defines β_D in Eq. (4.25c). As discussed in Sec. IV, the two values of the sign correspond to two different (but equally acceptable) trajectories in spacetime. A similar argument applies to the derivation of Eq. (5.9) from Eq. (5.6). Note that the square root in Eq. (5.6) is proportional to β_S, and the absence of spurious solutions follows from the fact that Eq. (4.27) provides a valid solution for either sign of β_S. Thus, the solutions to our problem are precisely the solutions to Eq. (5.9).

Note that the mass M occurs only in the variable E, and thus E (for $E<0$) characterizes the different solutions to the problem. The parameters of the underlying physics appear in the dimensionless parameter γ. If one assumes that the energy density of the false vacuum ρ_0 is of order $M_{\rm GUT}^4$, and that the surface energy density σ is of order $M_{\rm GUT}^3$, then taking $M_{\rm GUT} \approx 10^{14}$ GeV gives $\gamma \approx 10^{-4}$.

A graph of $V(z)$ is shown in Fig. 3. Although the physically plausible values of γ are very small, the graph is drawn for $\gamma = 1.3$ in order that the interesting features be large enough to see.

The important qualitative features of $V(z)$ hold for all values of γ. In particular, $V(z) \sim -1/z^4$ for small z, $V(z) \sim -z^2$ for large z, $V(z) < 0$ for all z, and $d^2V/dz^2 < 0$ for all z. $V(z)$ has one maximum at z_m, where

$$z_m{}^3 = \tfrac{1}{2}\{[8 + (1 - \tfrac{1}{2}\gamma^2)^2]^{1/2} - (1 - \tfrac{1}{2}\gamma^2)\} . \tag{5.12}$$

Figure 4 shows z_m as a function of γ. It can be seen (and it can be shown analytically) that $z_m > 1$ for any $\gamma^2 > 0$. The maximum value of the potential is given by

$$V_m = V(z_m) = -\frac{3(z_m{}^6 - 1)}{z_m{}^4} , \tag{5.13}$$

where the equation which determines z_m has been used to simplify the right-hand side.

There is critical mass defined by $E(M_{\rm cr}) = V_m$, given by

$$M_{\rm cr} = \overline{M} \frac{\gamma^3 z_m{}^6 (1 - \frac{1}{4}\gamma^2)^{1/2}}{3\sqrt{3}(z_m{}^6 - 1)^{3/2}} , \tag{5.14}$$

where

$$\overline{M} \equiv \frac{4\pi}{3} \chi^{-3} \rho_0 = \frac{1}{2G\chi} . \tag{5.15}$$

Note that $\overline{M}$ can be thought of as a characteristic mass for the problem, and is equal to ρ_0 times the volume of a Euclidean sphere with radius χ^{-1}. For $\rho_0 = (10^{14}\ \text{GeV})^4$, one has $\overline{M} \approx 3.1 \times 10^{28}$ GeV ≈ 56 kg. The factor which multiplies $\overline{M}$ in Eq. (5.14) approaches unity as $\gamma \to 0$, and the ratio $M_{\rm cr}/\overline{M}$ is shown as a function of γ in Fig. 5.

For $M < M_{\rm cr}$ (or equivalently, $E < V_m$), we distinguish two types of solutions. First, there are "bounded" solutions for which z starts at zero, grows to a maximum value for which $E = V(z)$, and then returns to $z=0$. Second, there are "bounce" solutions for which z approaches infinity in the asymptotic past, falls to a minimum value given by $E = V(z)$, and again approaches infinity in the asymptotic future. For $M > M_{\rm cr}$ the solu-

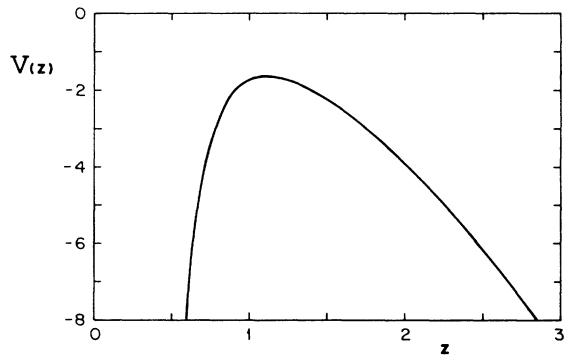

FIG. 3. A graph of the potential-energy function $V(z)$, for $\gamma = 1.3$.

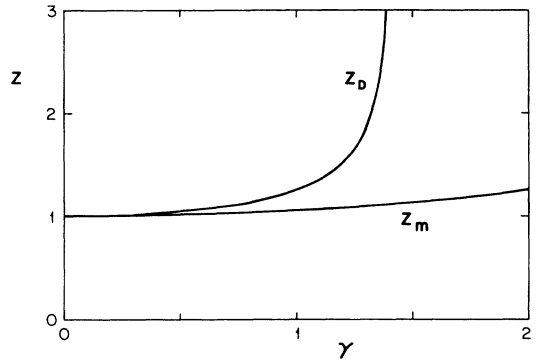

FIG. 4. Special values of z as a function of γ. The value of z which maximizes the potential energy is denoted by z_m, and the value at which β_D changes sign is denoted by z_D. The variable z has been defined so that β_S changes sign at $z=1$.

tions will be called "monotonic." The value of z starts at zero and then increases without bound. The time reversal of a monotonic solution is a distinct solution, while the time reversal of either a bounded or a bounce solution is indistinguishable from the original solution.

As a prelude of constructing spacetime diagrams for the bubble solutions, we will add some extra landmarks to Fig. 3. We will discuss these landmarks one at a time, and will show them on Fig. 6.

We begin by locating the values of z for which β_S and β_D change sign. Assuming that $\sigma>0$ we rewrite Eq. (5.1) as

$$\beta_S=\frac{1-z^3}{z^2\sqrt{|E|}} . \tag{5.16}$$

Thus, $\beta_S=0$ for $z=1$, $\beta_S>0$ for $z<1$, and $\beta_S<0$ for $z>1$. The mass M_S defined by $E(M_S)=V(z=1)$ is given by

$$M_S=\bar{M}(1-\tfrac{1}{4}\gamma^2)^{1/2} . \tag{5.17}$$

This formula is illustrated in Fig. 5. Similarly, using Eq. (4.27) one can show that

$$\beta_D=\frac{1-(1-\frac{1}{2}\gamma^2)z^3}{z^2\sqrt{|E|}} . \tag{5.18}$$

So if $\gamma^2<2$ (or equivalently if $\kappa^2<\chi^2$), then β_D changes sign when $z=z_D$, where

$$z_D=\frac{1}{(1-\frac{1}{2}\gamma^2)^{1/3}} . \tag{5.19}$$

If $\gamma^2\geq 2$ (or equivalently if $\kappa^2\geq\chi^2$) then β_D is always positive. Figure 4 shows z_D as a function of γ, and one can see (and it can be shown analytically) that $z_D>z_m$ for $0<\gamma^2<2$. The mass M_D defined by $E(M_D)=V(z_D)$ is given by

$$M_D=\bar{M}\frac{1-\frac{1}{2}\gamma^2}{1-\frac{1}{4}\gamma^2} , \tag{5.20}$$

a result which is plotted in Fig. 5. It can be seen (or shown analytically) that $M_D<M_S$ for $0<\gamma^2<2$.

Figure 6 also indicates the location of the horizon

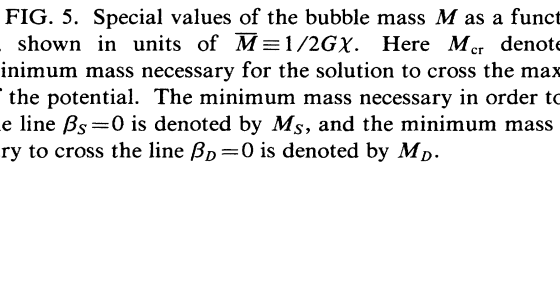

FIG. 5. Special values of the bubble mass M as a function of γ, shown in units of $\bar{M}\equiv 1/2G\chi$. Here M_{cr} denotes the minimum mass necessary for the solution to cross the maximum of the potential. The minimum mass necessary in order to cross the line $\beta_S=0$ is denoted by M_S, and the minimum mass necessary to cross the line $\beta_D=0$ is denoted by M_D.

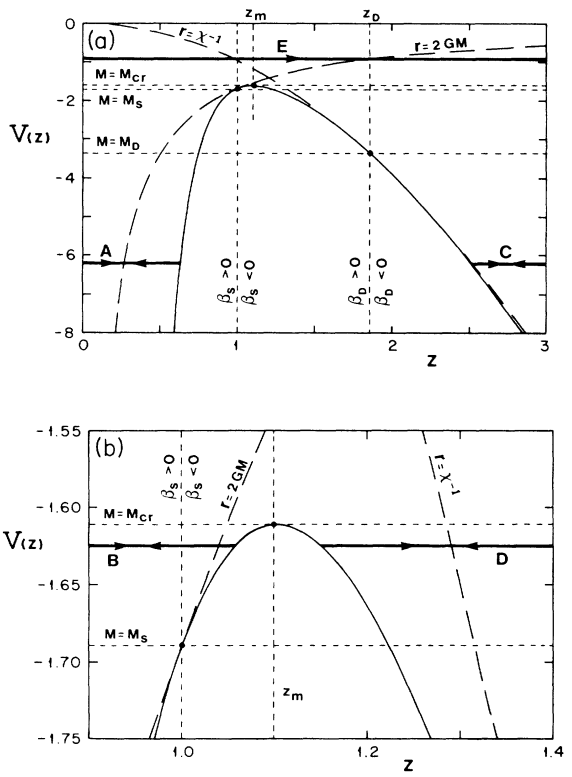

FIG. 6. Graph of the potential-energy function $V(z)$, for $\gamma=1.3$, shown with important landmarks. Part (a) shows a wide range of the variables, while part (b) shows a blow-up of the region around the peak of the potential. The figure shows the line $z=1$ at which β_S changes sign, and the line $z=z_D$ at which β_D changes sign. Broken horizontal lines indicate the values of E corresponding to M_{cr}, M_S, and M_D. The Schwarzschild horizon ($r=2GM$) and the de Sitter horizon ($r=\chi^{-1}$) are shown as broken lines. The solutions discussed in the text are shown, and are labeled by the letters A–E.

crossings. The Schwarzschild horizon $r=r_{SH}=2GM$ corresponds to

$$z_{SH}=\frac{\gamma^2}{|E|}\ . \tag{5.21}$$

In order to understand the behavior of this curve on Fig. 6, one may invert the relationship to obtain

$$E=-\frac{\gamma^2}{z_{SH}}=V(z_{HS})+\left[\frac{1-z_{SH}{}^3}{z_{SH}{}^2}\right]^2\ . \tag{5.22}$$

Thus the curve is tangent to the curve for $V(z)$ at $z=1$. Similarly, the de Sitter horizon $r=\chi^{-1}$ corresponds to

$$z_{DH}=\frac{\sqrt{|E|}}{\gamma(1-\frac{1}{4}\gamma^2)^{1/2}}\ . \tag{5.23}$$

The appearance of this function in Fig. 6 can also be better understood by inverting it, giving

$$\begin{aligned}E&=-\gamma^2 z_{DH}{}^2(1-\tfrac{1}{4}\gamma^2)\\&=V(z_{DH})+\frac{[(1-\frac{1}{2}\gamma^2)z_{DH}{}^3-1]^2}{z_{DH}{}^4}\ .\end{aligned} \tag{5.24}$$

This curve is tangent to the curve for $V(z)$ at $z=z_D$.

While Fig. 6 is quite complicated, it has the virtue that essentially all of the qualitative properties of the different types of solutions can be read directly from the diagram. Trajectories corresponding to each type of solution are marked with the letters A–E, and we will now discuss these solutions one at a time.

A. This is a bounded solution, corresponding to a small mass $M<M_S$. The variable r starts from zero and increases to a maximum value which is larger than the Schwarzschild radius, and then reverses its motion and returns to zero. During the entire trajectory both β_S and β_D are positive, which indicates that the polar angle in the Schwarzschild space coordinates is increasing, while the corresponding angle in the de Sitter space is decreasing. A diagram showing the behavior in each of these spacetimes is displayed as Fig. 7. The scale of the Schwarzschild diagram is small, because M is small and the line element for that spacetime has the form $ds^2=(2GM)^2 f(U,V)(-dV^2+dU^2)$. The value of the coordinate t at which the trajectory materializes is arbitrary, since the Schwarzschild manifold possesses the global symmetry $T\to T+\text{const}$. We have drawn the diagram with an initial t chosen to make it manifestly time-reversal ($V\to -V$) symmetric. The initial value of the de Sitter coordinate t can also be shifted by the symmetry operation $T\to T+\text{const}$, and again we have chosen conventions to display the time-reversal symmetry. These configurations are the black-hole solutions of Ipser and Sikivie[16] and Berezin, Kuzmin, and Tkachev.[17]

B. This is also a bounded solution, but lies in the narrow mass range $M_S<M<M_{cr}$. Again r increases from zero to a maximum value beyond the Schwarzschild radius, and then returns to zero. However, in this case the sign of β_S is negative while the trajectory is outside the Schwarzschild horizon, which means that the polar angle is decreasing. This implies that the trajectory goes through region III, rather than region I. A diagram of the spacetime behavior is shown in Fig. 8. In this figure and also the next two, the $T\to T+\text{const}$ symmetry has been used to achieve a manifest time-reversal symmetry. Note that this configuration allows the possibility of Schwarzschild observers in either region I or region III, both of whom are viewing the bubble from outside the Schwarzschild horizon. The observer in region I can see only the early stages of the evolution of the bubble, losing contact when the bubble-wall trajectory enters region III. A Schwarzschild observer in region III can follow the bubble wall through its history, but such an observer is doomed to collide with the future $r=0$ singularity. These configurations are the worm-hole solutions discussed by Berezin, Kuzmin, and Tkachev.[17]

C. This is a bounce solution, corresponding to a small mass $M<M_D$. These solutions will not exist at all if $\gamma^2>2$ (or equivalently if $\kappa^2>\chi^2$), in which case all bounce solutions will be of type *D*. In these solutions r starts at arbitrarily large values, decreases to a minimum which is inside the de Sitter horizon but outside the Schwarzschild horizon, and then increases again. The values of β_S and β_D are both negative, indicating that the Schwarzschild polar angle is decreasing, while the de Sitter polar angle is increasing. A spacetime diagram is shown in Fig. 9.

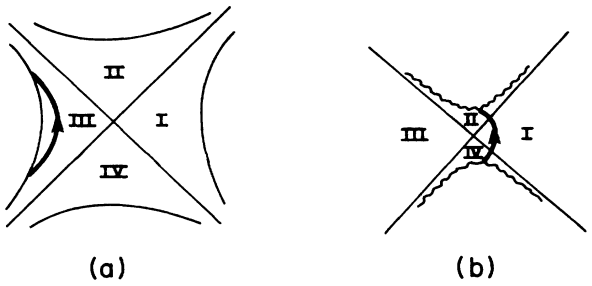

FIG. 7. Spacetime diagrams for a trajectory of type *A*. The trajectory in de Sitter space is shown in (a), and the trajectory in Schwarzschild space is shown in (b). The actual spacetime consists of the trajectory, those points in (a) to the left of it, and those points in (b) to the right of it. These are the bounded solutions for low values of the mass M, and they are called black-hole solutions.

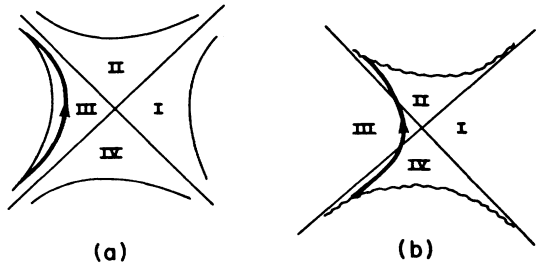

FIG. 8. Spacetime diagrams for a trajectory of type *B*, using the same conventions as in Fig. 7. These are called worm-hole solutions, and they are the bounded solutions for values of the mass which are larger than those of Fig. 7. Note that the bubble wall never enters region I of Schwarzschild space.

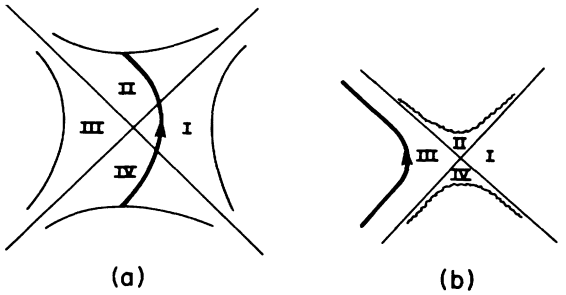

FIG. 9. Spacetime diagrams for a trajectory of type C. These are bounce solutions of low mass, and they exist provided that $\kappa^2 < \chi^2$. These solutions, as well as those illustrated in Figs. 10 and 11, have the possibility of producing an inflationary scenario.

Note that the trajectory enters both regions II and IV of the de Sitter diagram, and since it is timelike it must therefore reach both the lower and the upper boundaries. However, one must remember that these boundaries are not physical. They correspond to $r=\infty$, and an infinite proper time is required to reach them. Note also that the upper left-hand corner of the de Sitter space diagram describes a region of inflating de Sitter space which has all the properties of an inflationary universe. The diagram is drawn for an absolutely stable de Sitter space, but in appropriate particle theory models the false vacuum which permeates the de Sitter region would decay after an enormous amount of expansion. The latent heat released by this decay would reheat the region, producing a huge region of spacetime which would be indistinguishable by local measurements from a flat Friedmann-Robertson-Walker universe. Thus, if an initial configuration resembling a spacelike hypersurface in Fig. 9 could somehow be produced, then an acceptable inflationary scenario would result.

D. This is again a bounce solution, but this time in the mass range $M_D < M < M_{\rm cr}$. In this case the sign of β_D becomes positive before the trajectory crosses the de Sitter horizon, which indicates that it passes through region III rather than region I of the de Sitter diagram. A diagram of this spacetime appears in Fig. 10.

E. These are the monotonic solutions, for which r begins at zero and grows without bound. These trajectories occur only for $M > M_{\rm cr}$. The spacetime picture is shown in Fig. 11. Here we have used the symmetry $T \to T + \text{const}$ to ensure that the bubble materializes at $t=0$ in both the Schwarzschild and de Sitter coordinates. The initial value of β_S is positive, indicating that the trajectory in the Schwarzschild diagram must initially move toward the right. The sign of β_S reverses at the point marked Q in the diagram. The radius then grows beyond the Schwarzschild horizon with β_S negative, which implies that it enters region III. In the de Sitter diagram the configuration begins with β_D positive and $r=0$, which implies that it is in the region III. The sign of β_D changes at the point marked P, after the radius has surpassed the de Sitter horizon. Like the worm-hole configuration of type B, these configurations allow the possibility of Schwarzschild observers in either region I or region III. The observer in region I again sees only the earliest stages of the evolution of the bubble. The observer in region III finds himself between a Schwarzschild horizon at $R=2GM$ and a receding bubble wall at large values of R. He can in principle remain at a constant value of R if he chooses, he can catch up with the receding bubble wall and enter the de Sitter region, or he can allow himself to into the black hole. The inflationary region is in the upper left-hand corner of the de Sitter diagram. As discussed in the case of trajectories of type C, the decay of the false vacuum in this region can give rise to an acceptable inflationary scenario. However, we will see in Appendix D that solutions of this type exist even if $\chi=0$, and thus one cannot assume that these solutions are necessarily inflationary.

Since the monotonic solutions of type E seem the most interesting, we include several additional diagrams to help illustrate the nature of these configurations. Figure 12 shows a single spacetime diagram for the entire manifold, with several spacelike hypersurfaces indicated by the letters a–d. One can choose the coordinates of such a diagram to be the usual Kruskal-Szekeres coordinates in the Schwarzschild region, but one must then make a coordinate transformation[25] on the Gibbons-Hawking coordinates of the de Sitter space in order for the two halves of the diagram to fit smoothly together. Figure 13 is an attempt to picture this succession of spacelike hypersurfaces. We have suppressed one dimension, and have then embedded the resulting two-dimensional surface into a three-dimensional space in order to display its curvature. Note that hypersurface d corresponds to two disjoint spaces: one is a Schwarzschild space with a black-hole

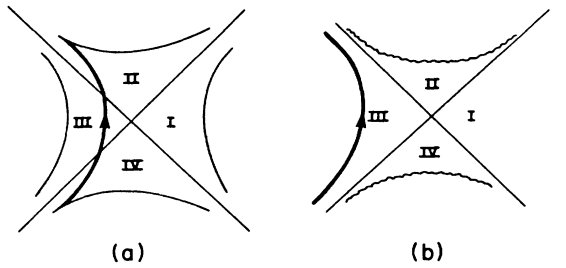

FIG. 10. Spacetime diagrams for a trajectory of type D. These are bounce solutions for values of the mass larger than those in Fig. 9. For $\kappa^2 > \chi^2$, all bounce solutions have this form.

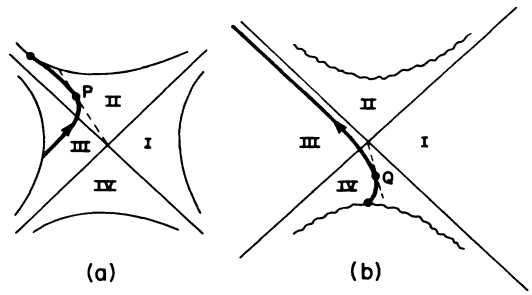

FIG. 11. Spacetime diagrams for a trajectory of type E. These are the monotonic solutions.

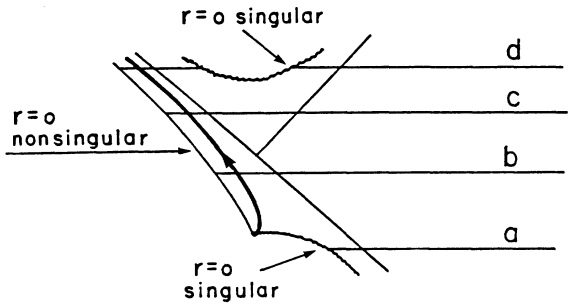

FIG. 12. The entire spacetime for the case of a monotonic bubble solution. Several constant V hypersurfaces are indicated for future reference by the letters $a-d$.

singularity at $r=0$, while the other is a closed universe which contains both de Sitter and Schwarzschild regions. It is the de Sitter region of the closed universe which inflates and which might ultimately produce the Friedmann-Robertson-Walker universe observed today.

In Fig. 13 one sees plainly how the two paradoxes discussed in the Introduction are avoided. The first paradox, concerning the volume of the false-vacuum region, is resolved when we consider the unusual geometric structure. The false-vacuum region inflates as expected, but it does not move outward into the true-vacuum region. In fact the domain wall is constantly accelerating in the direction of the false-vacuum region, but the false-vacuum region is inflating so quickly that the motion of the wall does not prevent its volume from increasing exponentially. The solution to the second paradox, concerning the radius of curvature of the domain wall, is also apparent in the figure. Observers next to the wall on either side would see its radius of curvature increase. The observer in the de Sitter region attributes this growth to the general inflation of his space; the observer in the Schwarzschild region, on the other hand, attributes it to the higher pressure of the true vacuum forcing the wall into the false-vacuum region, which lies at larger values of R.

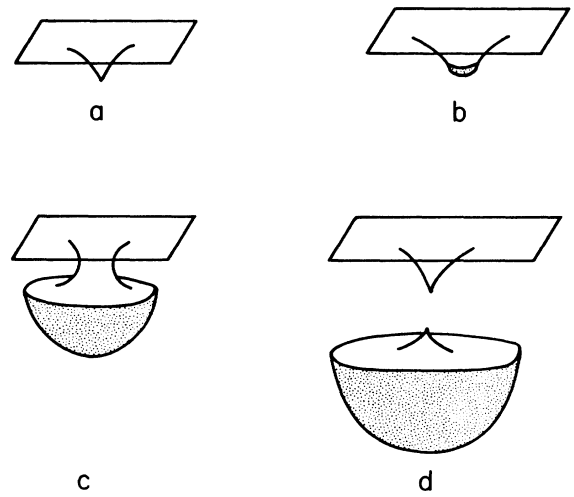

FIG. 13. The evolution of type E solutions. The three-dimensional spacelike hypersurface indicated in Fig. 12 are depicted by suppressing one dimension and embedding the resulting two-dimensional surface in a three-dimensional space. The de Sitter region is indicated by shading. In d one sees that the nascent inflationary universe (i.e., the de Sitter region) has detached from the original spacetime, and is now contained in an isolated closed universe which also contains a Schwarzschild region.

Our method of derivation guarantees that the solutions of types $A-E$ form an exhaustive set of solutions to the false-vacuum bubble equations of motion. On this point we are apparently in disagreement with Berezin, Kuzmin, and Tkachev,[18] who show a diagram (the second part of their Fig. 3) which does not resemble any of ours, and which we believe illustrates an impossible geometry.

For completeness we give in Appendix C the equations which determine the trajectories of the domain wall as seen in both the Kruskal-Szekeres and Gibbons-Hawking coordinates. This appendix also contains a discussion of the asymptotic behavior of those trajectories for which $r\rightarrow\infty$ as $\tau\rightarrow\infty$ (i.e., trajectories of types C, D, and E).

There are also some interesting special cases of these solutions, which are discussed in detail in Appendix D. First we examine the limit in which the surface energy density $\sigma\rightarrow 0$, and find that in this limit the domain-wall velocity approaches that of light, except at certain turnaround points. We then investigate a bounce solution which survives in the limit $M\rightarrow 0$, and we find it to be identical to the bounce solution found by Coleman and De Luccia.[26] The special case $\chi=0$ is not relevant to inflation, but it is interesting because it illustrates the gravitational repulsion of domain walls which was emphasized by Ipser and Sikivie.[16] For $\chi=0$ and $M=0$ there is a curious solution, found earlier by Ipser and Sikivie, which can be described as an inhomogeneous closed universe in which all of the energy density is concentrated in a domain wall which divides the universe in two. The repulsive gravity of the domain wall causes this universe to expand indefinitely.

VI. DISCUSSION AND CONCLUSIONS

In this paper we have analyzed the behavior of a spherically symmetric region of false vacuum which is separated from an infinite region of true vacuum by a domain wall. Several issues of cosmological interest may be viewed in a new light because of these results.

First there are the implications for the early universe. While some theories[27,28] predict an early universe which is very homogeneous, other approaches[29] describe an early universe which is highly chaotic. An important feature of the inflationary mechanism is that it allows for the possibility of such highly chaotic initial conditions. In a chaotic theory it is plausible that a region which inflates might be surrounded by regions that do not inflate, and one would like to understand the evolution of such a system. Assuming that our idealized spherically symmetric problem is indicative, one would expect that the inflating region would appear from the "outside" (i.e., from region I of the Schwarzschild manifold) as a black hole, and essentially all of the inflation would take place in the causally disconnected region III. The inflating region

would then detach completely from the manifold which spawned it, forming an isolated closed universe. Sato, Kodama, Sasaki, and Maeda[11] have previously pointed out that such isolated closed universes can be produced, and they have called them "child universes." We have illustrated several snapshots of the evolving system in Fig. 13, where we have used the Kruskal-Szekeres coordinate V as the time variable. The isolated closed universe seen in the final snapshot consists of two regions, as may be seen in Fig. 13, hypersurface d. The first consists of false vacuum which soon decays into thermal radiation, producing a huge region which behaves as a standard Friedmann-Robertson-Walker universe. The other region is an essentially empty Minkowski space, with a Schwarzschild black hole in the center. The black hole evaporates by emitting Hawking radiation. The evaporation rate depends inversely on the cube of the black-hole mass, so that a sufficiently light black hole can evaporate very quickly.

Since the detachment of an isolated closed universe is a significant feature of the solution, it is important to consider the extent to which this description depends on the choice of spacetime slicing. Let us for the moment ignore the possibility of black-hole evaporation. The future singularity of Schwarzschild space lies on a spacelike hypersurface, and it is therefore possible to choose equal-time slices which approach the singularity without ever reaching it—in such a coordinate system, the manifold would remain connected at all times. Thus, the connectedness of the equal-time hypersurfaces depends on the choice of slicing. This situation is different from that in Minkowski space, in which the equal-time hypersurfaces are always connected, but it is similar to that in de Sitter space or in Schwarzschild space. In any case, the closed universe is "detached" in the sense that it is causally disconnected. An observer living in the closed universe will never be able to travel to, or send messages to, the exterior Schwarzschild space (region I).

If, on the other hand, we assume that black-hole evaporation takes place and proceeds to completion, then the detachment of the child universe can be stated unequivocally, as has been pointed out by Sato, Kodama, Sasaki, and Maeda.[11] From region I (exterior Schwarzschild space) one sees a black hole in empty space, and its evaporation would cause the line of singularity to terminate at a spacetime point which is shown as P in Fig. 14. At this point the spacelike, singular $r=0$ line becomes nonsingular and continues in a future timelike direction. The fate of the black hole as seen from region III (interior of the false-vacuum bubble) is more complicated, since this black hole is exposed to the Gibbons-Hawking radiation[23] of the de Sitter space. For solutions with $M \approx \overline{M}$ [see Eq. (5.15)], the Gibbons-Hawking temperature $T_{\rm GH}=\chi/2\pi$ of the de Sitter space is twice as high as the Hawking temperature $T_H=1/8\pi GM$ of the black hole, and thus the black hole would be expected to accrete rather than evaporate. However, in an inflationary scenario the false vacuum is not absolutely stable, and will eventually decay. At that time the region enters a Friedmann-Robertson-Walker phase, cooling as the expansion continues. Soon the black hole will find itself in a relatively cold environment, and then evaporation will take place. The spacetime point at which the evaporation is completed is shown in Fig. 14 as $\tilde{P}$. We further let R denote the interior of the future light of P, and $\tilde{R}$ denote the interior of the future light cone of $\tilde{P}$. In this case one can say unambiguously that the space has disconnected, in the following sense: any path from a point in R to a point in $\tilde{R}$ must include segments traveling in *both* the past timelike and future timelike directions. This implies that there exists no possible slicing of spacetime which allows the manifold to remain connected. (Note, by the way, that we must make use of both evaporation events P and $\tilde{P}$ in constructing the above argument. If, for example, the evaporation at $\tilde{P}$ is assumed not to take place, then the spacetime diagram can be compactified as shown in Fig. 15. In this case one can choose a slicing in which the space remains connected, but in which the interior of the false-vacuum bubble has ceased to exist by the time of event P.)

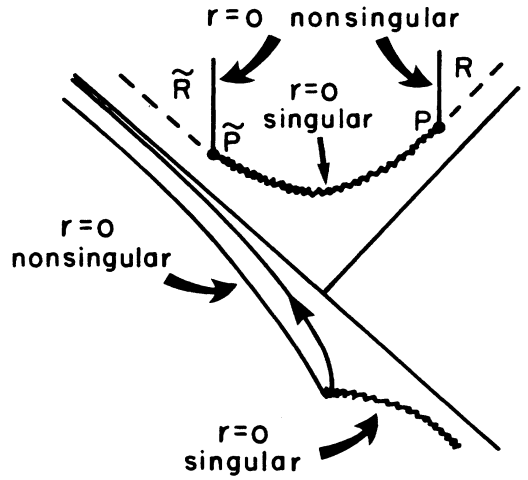

FIG. 14. Spacetime diagram for a monotonic bubble solution, including black-hole evaporation. Under these assumptions the detachment of the false-vacuum bubble becomes unequivocal.

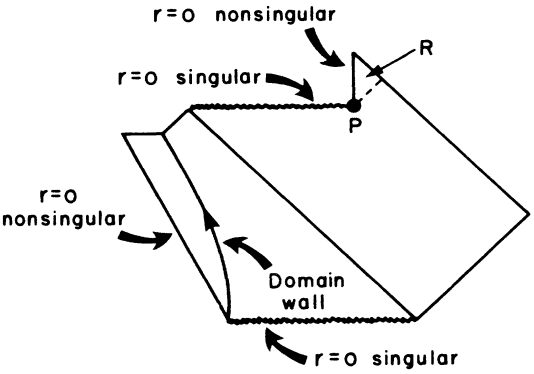

FIG. 15. Compactified spacetime diagram for monotonic bubble solution, including black-hole evaporation in the Schwarzschild region only. In this case one can choose a slicing in which the space remains connected.

Work is currently in progress[30] to determine whether or not it is possible in principle[31] to produce an inflationary universe in the laboratory (i.e., by man-made processes). Each of the exact solutions for inflationary bubbles described in Sec. V begins with an initial singularity, a feature which has to be avoided if one is to produce such an object in the laboratory. Thus, one must ask whether some method of intervention can be used to produce the same final state from a different initial state.[32] It seems to us that an arbitrarily low initial mass density is one criterion that an acceptable "laboratory" state must satisfy. The extraordinary mass densities involved in the inflationary solutions should be developed by concentrating low density matter from a much larger region. The difficulty stems from the fact that the standard picture of the gravitational collapse of ordinary matter produces the situation shown in Fig. 16, which is quite different from the inflationary solution shown in Fig. 12. In particular, the standard picture of gravitational collapse does not lead to the full future singularity as seen in the inflationary solution.

The challenge, then, is to determine whether it is possible to set up as an initial condition the configuration corresponding to a nonsingular spacelike hypersurface of the exact solution, such as the hypersurfaces marked b or c in Fig. 12. Note that there is no topological barrier to constructing such an initial condition, since Fig. 13 shows clearly that these hypersurfaces are topologically equivalent to Euclidean three-space. However, it can be shown,[30] at least in the case of exact spherical symmetry, that the initial singularity cannot be avoided. The proof makes use of the Penrose theorem, which relies on the assumption that the energy-momentum tensor obeys the weak energy condition (i.e., that $T_{\mu\nu}\eta^{\mu}\eta^{\nu}\geq 0$ for any timelike or null vector η^{μ}). Intuitively, the result indicates that the outward velocity required for the monotonic solutions is so large that it can emerge only from an initial singularity.

Our results suggest the possibility that an inflationary universe could be created by quantum-mechanical tunneling from a Minkowski space. To see how this might occur, note that Minkowski space is not an eigenstate of the energy density operator. Although the total energy of the Minkowski space is zero, the mean energy density in any given region is constantly fluctuating between positive and negative values, with the average at zero. Thus, the weak energy condition is violated at the quantum level, and the theorem described in the previous paragraph does not apply. It is conceivable that a local region could fluctuate into a high-energy false-vacuum state, producing a situation similar to that shown as hypersurface b or c in Fig. 13. The region could then evolve temporarily according to the classical evolution shown in Fig. 13, resulting in a closed inflationary universe which disconnects from the original Minkowski space. The Minkowski space is then left with a virtual black hole, which soon disappears by Hawking evaporation. For a black hole with a mass of order $M\approx 10^{28}$ GeV as expected for this kind of process, the time scale for Hawking evaporation is given by $M^3/M_P{}^4\approx 10^{-14}$ sec. Thus, the net result is an initial Minkowski space which tunnels to become a final Minkowski space plus a closed inflationary universe. It seems clear that no conservation laws are violated in this hypothetical process. The possibility of such tunneling remains for now a matter of speculation, but perhaps further work can clarify the situation.[33]

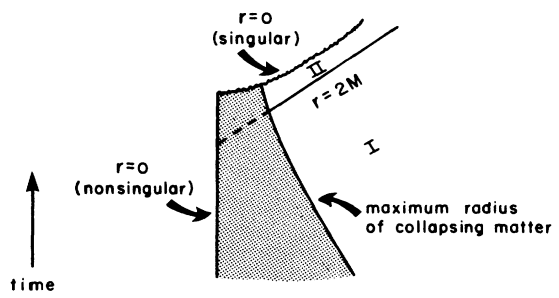

FIG. 16. Spacetime diagram illustrating the collapse of ordinary matter.

If an inflationary universe can be created by tunneling from Minkowski space, then the process may be a key step in a solution to the cosmological constant problem. Abbott[34] has recently proposed a model which, given some assumptions about the underlying particle physics, explains how the universe could evolve into a huge region of very nearly Minkowskian spacetime. The idea of remaining for a long time in a Minkowski space seems to be an attractive feature for any scheme which solves the cosmological constant problem by dynamical relaxation, since it is hard to see how the delicate cancellations required to fix the cosmological constant could be the result of processes which take place at high energy. However, in order to make such a scenario workable, one must have a mechanism for producing an acceptable universe from a Minkowski space. The tunneling process described above may provide such a possibility.

Finally, the results obtained here are possibly relevant to the question of whether or not information is irretrievably lost in a black hole. At the classical level it is clear that the loss of information is irreversible, but some authors[35] have argued that this information might be returned to the external spacetime during the process of black-hole evaporation. If, however, a repository for information is created by the detachment of a false-vacuum bubble, then the argument for the irretrievable loss of information would be strengthened. Note, however, that for the exact solutions described by Fig. 12, all of the information in the false-vacuum bubble originates in the initial singularity, and none comes for the external Schwarzschild region. Thus, while the notion of a detaching false-vacuum bubble may prove relevant in considerations of information loss, the exact spherically symmetric solutions that have been studied so far do not show any evidence for this effect.

ACKNOWLEDGMENTS

It is a pleasure to acknowledge useful discussions with Jim Bardeen, Edward Farhi, Werner Israel, Richard Matzner, Malcolm Perry, William Press, William Unruh, and Robert Wald. We would like to express our appreciation of the early work on this problem done by Neil

Woodward and José Figueroa-O'Farrill, and we would like to thank Gary Steigman and Ian Redmount for calling our attention to the work of Sato *et al.* The work of S.K.B. and E.I.G. was supported in part through funds provided by the U.S. Department of Energy (DOE) under Contract No. DE-AC02-76ERO3069. The work of A.H.G. was supported in part through funds provided by the U.S. Department of Energy (DOE) under Contract No. DE-AC02-76ERO3069, in part by the National Aeronautics and Space Administration (NASA) under Grant No. NAGW-553, and in part by the Alfred P. Sloan Foundation.

APPENDIX A: THE FORCE ON A THIN WALL

In Sec. III we applied energy-momentum conservation to the singular expression for $T^{\mu\nu}$ which is applicable to the thin-wall approximation, and we found an ambiguous expression in Eq. (3.6). As was pointed out in the text, the problem arose because we were computing the gravitational force on a sheet of mass, a situation which is completely analogous to the elementary problem of evaluating the electrostatic force on a sheet of charge. In this appendix we will show that the ambiguity can be resolved by methods very similar to those used in the electrostatics case, with a result which is also very similar.

The problem arises when one evaluates the integral

$$I \equiv \int_{-\epsilon}^{\epsilon} d\eta\, K^i{}_j T^j{}_i \tag{A1}$$

which appears when one tries to extract the consequences of Eq. (3.1b) for the behavior of the wall. When evaluated naively with the δ-function expression (3.2) for $T^{\mu\nu}$, the expression is ambiguous because, according to Eq. (2.12), $K^i{}_j$ is discontinuous at the bubble wall ($\eta=0$). Equation (A1) is analogous to the expression $\int d\eta\, E_\eta \rho$ which expresses the normal component of the electrostatic force on a charged sheet.

To evaluate (A1), one needs information about how $K^i{}_j$ varies as one crosses the domain wall, and this information is contained in Eq. (2.8c). Only the singular terms are important at the wall, so

$$\partial_\eta(K^i{}_j - \delta^i{}_j \mathrm{Tr}K) = -8\pi G T^i{}_j(\text{singular}) , \tag{A2}$$

which is analogous to $\partial_\eta E_\eta = 4\pi\rho$ in electrostatics.

Thus

$$I = -\frac{1}{8\pi G} \int_{-\epsilon}^{\epsilon} d\eta\, K^i{}_j \partial_\eta (K^j{}_i - \delta^j{}_i \mathrm{Tr}K) . \tag{A3}$$

Straightforward manipulations then lead to the result

$$I = \overline{K}^i{}_j \int_{-\epsilon}^{\epsilon} d\eta\, T^j{}_i , \tag{A4}$$

where $\overline{K}^i{}_j$ is defined by Eq. (3.7).

APPENDIX B: COORDINATE SYSTEMS FOR DE SITTER SPACE

This appendix shows the relationship between the Gibbons-Hawking[23] coordinate system for de Sitter space and several better-known coordinate systems.

Probably the most transparent way to think of de Sitter space is to embed it in a five-dimensional space with coordinates u^α, where $\alpha = 1, \ldots, 5$ and the metric is given by

$$\eta_{\alpha\beta} = \mathrm{diag}[1,1,1,1,-1] . \tag{B1}$$

de Sitter space is given by the subspace satisfying $u^2 = 1/\chi^2$, with the line element $ds^2 = \eta_{\alpha\beta} du^\alpha du^\beta$. The Gibbons-Hawking coordinates can be related to these by

$$U = \frac{\chi u^4}{1+\chi r}, \quad V = \frac{\chi u^5}{1+\chi r} , \tag{B2}$$

where

$$r^2 \equiv |\mathbf{u}|^2 \equiv \sum_{i=1}^{3} (u^i)^2 . \tag{B3}$$

The coordinates θ and ϕ are simply the usual polar angles associated with the three-vector $\mathbf{u}$.

Another well-known choice is the Robertson-Walker flat coordinate system $(t,\mathbf{x})$, with line element

$$ds^2 = -dt^2 + e^{2\chi t} d\mathbf{x}^2 . \tag{B4}$$

These coordinates are related to the five-dimensional system by

$$\begin{aligned} t &= \chi^{-1} \ln[\chi(u^4+u^5)] , \\ x^i &= \frac{u^i}{\chi(u^4+u^5)} . \end{aligned} \tag{B5}$$

In terms of the Robertson-Walker flat coordinates, the Gibbons-Hawking coordinates can be expressed as

$$\begin{aligned} U &= \frac{\cosh\chi t - \frac{1}{2}\chi^2 \mathbf{x}^2 e^{\chi t}}{1+\chi|\mathbf{x}|e^{\chi t}} , \\ V &= \frac{\sinh\chi t + \frac{1}{2}\chi^2 \mathbf{x}^2 e^{\chi t}}{1+\chi|\mathbf{x}|e^{\chi t}} . \end{aligned} \tag{B6}$$

The coordinates θ and ϕ are the polar angles of the three-vector $\mathbf{x}$.

Finally we consider the Robertson-Walker closed coordinate system (T,Ψ,θ,ϕ), with line element

$$ds^2 = -dT^2 + \chi^{-2}\cosh^2\chi t (d\Psi^2 + \sin^2\Psi\, d\Omega^2) . \tag{B7}$$

These coordinates are related to the five-dimensional system by

$$\begin{aligned} T &= \chi^{-1} \mathrm{arcsinh}(\chi u^5) , \\ \Psi &= \arctan(|\mathbf{u}|/u^4) . \end{aligned} \tag{B8}$$

In terms of these coordinates, the Gibbons-Hawking coordinates can be written as

$$\begin{aligned} U &= \frac{\cosh\chi t \cos\Psi}{1+\cosh\chi t \sin\Psi} , \\ V &= \frac{\sinh\chi t}{1+\cosh\chi t \sin\Psi} , \end{aligned} \tag{B9}$$

and the angles θ and ϕ are the same in the two systems.

APPENDIX C: THE SPACETIME TRAJECTORY OF THE DOMAIN WALL

In this appendix we give the equations which define the spacetime trajectory of the domain wall as seen in either

Kruskal-Szekeres or Gibbons-Hawking coordinates. We assume that the trajectory function $r(\tau)$ has already been found by solving Eq. (5.9). The spacetime trajectory will of course not be unique, since both the Schwarzschild space and the de Sitter space possess symmetries of the form $T \rightarrow T + \text{const}$.

Beginning with the Kruskal-Szekeres coordinates, one has from Eq. (4.4) the relation

$$u^2 - v^2 = \left[\frac{r}{2GM} - 1 \right] e^{r/2GM} . \tag{C1}$$

To construct the spacetime trajectory, choose any initial proper time τ_0. Then choose initial coordinates $u(\tau_0)$ and $v(\tau_0)$ consistent with Eq. (C1), and chosen in the proper quadrant. Differentiation of Eq. (C1) provides an equation involving $\dot{u}$ and $\dot{v}$, and Eq. (4.18b) provides another. The solution to these two simultaneous equations is given by

$$\begin{aligned} \dot{v} &= \frac{1}{4GM} \left[1 - \frac{2GM}{r} \right]^{-1} (u\beta_S + v\dot{r}) , \\ \dot{u} &= \frac{1}{4GM} \left[1 - \frac{2GM}{r} \right]^{-1} (v\beta_S + u\dot{r}) . \end{aligned} \tag{C2}$$

Although the equations contain an apparent singularity at $r = 2GM$, it can be seen by careful inspection that this singularity is canceled by the vanishing of the factors $(u\beta_S + v\dot{r})$ and $(v\beta_S + u\dot{r})$. Thus, the spacetime trajectory of the domain wall in Kruskal-Szekeres coordinates can be obtained by integrating Eqs. (C2).

From these equations one can understand the asymptotic behavior of those trajectories for which $r \rightarrow \infty$ as $\tau \rightarrow \infty$ (i.e., trajectories of types C, D, and E). From Eq. (5.9) one can see that $V(z) \approx -z^2$ for large z, which implies that $z(\tau') \propto e^{\tau'}$ for large τ'. Thus, $r(\tau) \propto e^{\chi_+^2 \tau / 2\kappa}$. Using Eq. (4.18c) one then has

$$\beta_S \rightarrow -\dot{r} - \frac{1}{2\dot{r}} + \cdots , \tag{C3}$$

where the overall sign was determined in Sec. V. If we define $w \equiv u + v$, then Eqs. (C2) imply that asymptotically

$$\frac{\dot{w}}{w} = -\frac{1}{8GM\dot{r}} . \tag{C4}$$

Since the integral of the right-hand side approaches a constant as $\tau \rightarrow \infty$, it follows that $\ln(-w)$ approaches a finite nonzero constant. This implies that, on the Kruskal-Szekeres diagram, the trajectory asymptotically approaches a line which is parallel to the horizon ($R = 2GM$) line. Thus the trajectory of the domain wall, as seen by an observer in the true-vacuum region, is asymptotically lightlike.

The asymptotic behavior of the trajectory can also be described in terms of the proper acceleration of the domain wall, defined by

$$\alpha \equiv \xi_\mu \frac{DU^\mu}{D\tau} . \tag{C5}$$

According to Eq. (3.18) this is just the negative of the extrinsic curvature component $K_{\tau\tau}$, which can be expressed in terms of $r(\tau)$ by using Eq. (4.28). One finds that asymptotically the domain wall approaches a uniform proper acceleration

$$\alpha_S \rightarrow -\frac{\chi_+^2}{2\kappa} , \tag{C6}$$

where the subscript S has been appended to indicate that we are discussing the proper acceleration as measured by an observer in the Schwarzschild region. We have defined ξ_μ to point from the de Sitter region to the Schwarzschild region, so the minus sign in Eq. (C6) indicates that the actual proper acceleration is toward the de Sitter region.

The procedure for obtaining the equations in Gibbons-Hawking coordinates is identical to that used for the Kruskal-Szekeres coordinates. Equations (C1) and (C2) are replaced by

$$u^2 - v^2 = \frac{1 - \chi r}{1 + \chi r} \tag{C7}$$

and

$$\begin{aligned} \dot{v} &= -\chi(1 - \chi^2 r^2)^{-1} (u\beta_D + v\dot{r}) , \\ \dot{u} &= -\chi(1 - \chi^2 r^2)^{-1} (v\beta_D + u\dot{r}) . \end{aligned} \tag{C8}$$

From these equations one can determine the asymptotic form of the domain-wall trajectory as seen by an observer in the de Sitter region, and the results are quite a bit different from the previous case. Using Eq. (4.25c) one finds that

$$\beta_D \rightarrow -\left[\frac{\chi^2 - \kappa^2}{2\kappa} \right] r + \cdots , \tag{C9}$$

where again the sign has been determined in Sec. V. It follows that

$$\begin{aligned} \dot{v} &\rightarrow \frac{1}{2\kappa\chi r} [(\chi^2 + \kappa^2)v - (\chi^2 - \kappa^2)u] , \\ \dot{u} &\rightarrow \frac{1}{2\kappa\chi r} [(\chi^2 + \kappa^2)u - (\chi^2 - \kappa^2)v] . \end{aligned} \tag{C10}$$

Figures 9–11 show that these trajectories asymptotically approach finite values of u and v (satisfying the relation $v^2 - u^2 = 1$), and thus the asymptotic value of the slope $dv/du = \dot{v}/\dot{u}$ can approach any value between -1 and 1.

The de Sitter observer also concludes that the domain wall approaches a uniform proper acceleration, which is found to be

$$\alpha_D \rightarrow -\left[\frac{\chi^2 - \kappa^2}{2\kappa} \right] . \tag{C11}$$

Again the acceleration points into the de Sitter region (provided that $\chi^2 > \kappa^2$). However, in de Sitter space a uniform proper acceleration does not imply that the trajectory is asymptotically lightlike. In fact, in any Robertson-Walker coordinate system the trajectory approaches a limiting velocity which is less than that of light. (This claim may at first seem bizarre, since each comoving Robertson-Walker observer must see the domain wall accelerate as it passes. However, the observer would also see his fellow comoving observers accelerate away from him-

self, and the domain wall would maintain a uniform velocity relative to the comoving observers that it passes.) To derive the asymptotic velocity, we write the general Robertson-Walker line element for de Sitter space as

$$ds^2=-dt^2+a^2(t)[d\psi^2+r^2(\psi)d\Omega^2]\ , \tag{C12}$$

where

$$a(t)=\begin{cases}\chi^{-1}\cosh\chi t & \text{if } k=1\ ,\\ \frac{1}{2}\chi^{-1}e^{\chi t} & \text{if } k=0\ ,\\ \chi^{-1}\sinh\chi t & \text{if } k=-1\ ,\end{cases} \tag{C13}$$

and

$$r(\psi)=\begin{cases}\sin\psi & \text{if } k=1\ ,\\ \psi & \text{if } k=0\ ,\\ \sinh\psi & \text{if } k=-1\ .\end{cases} \tag{C14}$$

We are using here an unconventional normalization for $a(t)$ in the $k=0$ case, but is is convenient for our purposes that the behavior of $a(t)$ for large t be independent of k. After some algebra we find that the proper acceleration of a trajectory in the radial direction is given in these coordinates by

$$\alpha=\frac{1}{a}\frac{d}{dt}\left[\frac{a^2\psi'}{(1-a^2\psi'^2)^{1/2}}\right]\ , \tag{C15}$$

where the prime denotes a derivative with respect to t. Since $a\psi'=1$ for a lightlike trajectory, its value for any other trajectory is interpreted as the velocity in units of the speed of light. Using the asymptotic relation $a(t)\rightarrow\frac{1}{2}\chi^{-1}e^{\chi t}$ which holds for any k, one can show that $a\psi'$ asymptotically approaches a constant:

$$\text{velocity}=a\psi'\rightarrow\frac{\alpha}{(\chi^2+\alpha^2)^{1/2}}\ . \tag{C16}$$

With the proper acceleration given by Eq. (C11), the asymptotic velocity of the domain wall is found to be

$$\text{velocity}\rightarrow\frac{\chi^2-\kappa^2}{\chi^2+\kappa^2}\ . \tag{C17}$$

The asymptotic velocity of the domain wall has also been studied by Berezin, Kuzmin, and Tkachev,[17] who considered the more general case in which the true-vacuum energy density might be nonzero. Their formula for the asymptotic velocity reduces to Eq. (C17) for the appropriate special case, but the words which accompany their formula are not sufficiently detailed for us to tell if we are in complete agreement. In our analysis this asymptotic velocity applies only to observers in the de Sitter region who use a Robertson-Walker coordinate system, but Berezin, Kuzmin, and Tkachev, do not state these limitations.

APPENDIX D: SOLUTIONS FOR SPECIAL CASES

In this appendix we discuss some interesting special cases of the general class of solutions described in Sec. V.

First, we consider the limit in which the surface energy density $\sigma\rightarrow0$, in which case $\gamma\rightarrow0$ also. As discussed at the beginning of Sec. V, typical grand unified theories give values of γ which are near to this limit ($\gamma\approx10^{-4}$).

In this limit the maximum of the potential $V(z)$ moves to $z_m=1$, with $V_m=0$. For any fixed value of M, E will approach zero in the limit. Equation (5.9) is then easily solved, giving

$$z^3=1\pm ce^{\pm3\tau'}\ , \tag{D1}$$

where the two sign choices can be made independently, and c is an arbitrary constant. According to Eq. (5.5) the relation between τ and τ' becomes singular in this limit, which means that $\dot r\equiv dr/d\tau$ approaches infinity, except in the vicinity of $z=1$. Thus, the domain-wall velocity approaches that of light.

Figure 5 shows that in this limit $M_{\rm cr}$, M_S, and M_D all approach $\overline{M}$. Solutions of type A or C are then possible if $M<\overline{M}$, and a solution of type E is possible if $M>\overline{M}$. The spacetime diagrams for these solutions can be constructed from Figs. 7, 9, and 11 by replacing the curved line segments by straight lines at 45° to the vertical. (A formal proof that the lines must approach 45° for $z\neq1$ can be constructed from the equations of Appendix C.) The line segments are then joined by sharp bends of 90°, which are located at points corresponding to $z=1$.

The limit $\sigma\rightarrow0$ has also been investigated by Aurilia, Denardo, Legovini, and Spallucci,[19] but we disagree with their results. They found only the static solution which corresponds in our language to $z(\tau')=1$, and they failed to notice that this solution is unstable. The error in their analysis, in our opinion, is that they ignored the possibility that $\dot r$ could diverge in the limit $\sigma\rightarrow0$.

Next, we consider the limit $M\rightarrow0$. It can be seen from Fig. 6 that in this limit the only solutions will have very small or very large values of z.

For the case of small values of z, the solutions are of type A and $V(z)$ can be approximated by $-1/z^4$. These solutions have a maximum radius, and it is easy to show that it is given by

$$r_{\max}\rightarrow\sqrt{GM/\kappa} \tag{D2}$$

as $M\rightarrow0$. Thus, these solutions become trivial in the limit.

For the case of large values of z, the solutions will be of type C or D depending on whether κ^2 is less than or greater than χ^2, respectively. In either case one can approximate $V(z)$ by $-z^2$, and one finds the exact solution

$$r(\tau)=\frac{2\kappa}{\chi_+^{\,2}}\cosh\left[\frac{\chi_+^{\,2}\tau}{2\kappa}\right]\ . \tag{D3}$$

To understand the spacetime structure, note that regions II and IV of the Schwarzschild space disappear as $M\rightarrow0$. In this limit regions I and III become Minkowski spaces, and the bridge which normally connects them disappears. Thus in the $M\rightarrow0$ limit either of the regions I or III of the Schwarzschild space constitutes a complete solution to the Einstein equations. In our case, the nontrivial solution is obtained by deleting region I of Schwarzschild space, and one then has a closed space consisting of a

Minkowski region and a de Sitter region. This closed space is precisely the thin-wall solution found by Coleman and De Luccia,[26] and Eq. (D3) above is equivalent to their result.

The special case $\chi=0$ is of course not relevant to inflation, but it does serve to illustrate the repulsive gravitational properties of domain walls which were emphasized by Ipser and Sikivie.[16] As $\chi\to 0$, one can see from Eqs. (5.14) and (5.17) that both $M_{\rm cr}$ and M_S have finite limits, given by $16/(27G\kappa)$ and $1/(2G\kappa)$, respectively. In this limit one has $\gamma=2$, so β_D is positive for all values of z. Thus, solutions exist of types A, B, D, and E. For types D and E the radius variable r will grow without bound at large times. The behavior of type D or E solutions at large times can be illustrated by Fig. 17, which is similar to hypersurface d of Fig. 13 except that the de Sitter region has been replaced by a section of flat space. The isolated closed space at the lower part of the picture will grow indefinitely, driven by the repulsion of the domain wall. The limit $M\to 0$ (keeping $\chi=0$) has also been investigated by Ipser and Sikivie. In this case the only nontrivial solutions are of type D, and Eq. (D3) reduces to $r(\tau)=(2/\kappa)\cosh(\kappa\tau/2)$. The spacetime geometry can be thought of as a limiting case of the Coleman–De Luccia bubble discussed above. Again there is a Minkowski region (region I of Schwarzschild space) which becomes disconnected as $M\to 0$, and this region can be deleted from the solution. One then has a closed space composed of two compact spherical regions of flat space, joined together at the domain wall. This is the "class-I" solution of Ipser and Sikivie, and can be described as an inhomogeneous closed universe in which all the energy density is concentrated in a domain wall at the operator. While the positive-energy theorem often implies that Minkowski space is the only solution for $M=0$, the theorem is evaded by this case because the manifold is not asymptotically flat.

"Vacuum shells" with $M=0$ were discussed by Berezin, Kuzmin, and Tkachev,[17] but their conclusions do not completely coincide with ours. We agree with their statement that these bubbles have a point of rest and expand infinitely, and the formula which they give for the minimum radius reduces to ours for the case in which the true-vacuum energy density is set equal to zero. However, they conclude that such domains could exist in our universe until now without conflicting with observational data, due to $M=0$. From our point of view, the discussion of this situation would depend on where "our universe" was assumed to lie. Our universe could lie in region III of the Schwarzschild space diagrams of Figs. 9 or 10, in which case we would be surrounded by a single domain wall which would be accelerating away from us. Alternatively, our universe could be in region I, but then the domain wall would lie in a completely disconnected region of spacetime. The region of the domain wall would be topologically connected to our region if M were small but nonzero, but the region would still be causally disconnected.

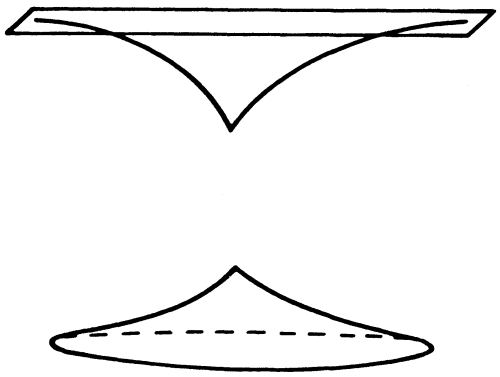

FIG. 17. The large-time behavior of solutions of types D or E, for the special case $\chi=0$.

*Present address: Department of Physics, University of Texas, Austin, TX 78712.
†Present address: Department of Physics, Ben-Gurion University, P.O.B. 653, 84 105 Beer-sheva, Israel.

[1]A. H. Guth, Phys. Rev. D **23**, 347 (1981).
[2]A. D. Linde, Phys. Lett. **108B**, 389 (1982).
[3]A. D. Linde, Phys. Lett. **114B**, 431 (1982).
[4]A. Albrecht and P. J. Steinhardt, Phys. Rev. Lett. **48**, 1220 (1982).
[5]A. A. Starobinsky, Phys. Lett. **117B**, 175 (1982).
[6]A. H. Guth and S.-Y. Pi, Phys. Rev. Lett. **49**, 1110 (1982).
[7]S. W. Hawking, Phys. Lett. **115B**, 295 (1982).
[8]J. M. Bardeen, P. J. Steinhardt, and M. S. Turner, Phys. Rev. D **28**, 679 (1983).
[9]R. Brandenberger, R. Kahn, and W. H. Press, Phys. Rev. D **28**, 1809 (1983).
[10]R. Brandenberger and R. Kahn, Phys. Rev. D **29**, 2172 (1984).
[11]K. Sato, H. Kodama, M. Sasaki, and K. Maeda, Phys. Lett. **108B**, 103 (1982).
[12]K. Sato, M. Sasaki, H. Kodama, and K. Maeda, Prog. Theor. Phys. **65**, 1443 (1981); H. Kodama, M. Sasaki, K. Sato, and K. Maeda, *ibid.* **66**, 2052 (1981); K. Sato, *ibid.* **66**, 2287 (1981); H. Kodama, M. Sasaki, and K. Sato, *ibid.* **68**, 1979 (1982).
[13]A. H. Guth and E. J. Weinberg, Nucl. Phys. **B212**, 321 (1983) have shown that such trapped regions of false vacuum are highly improbable in the context of the original inflationary model. The enormous diversity in the sizes of true-vacuum bubbles makes it very unlikely to have any configuration which includes two or more true-vacuum bubbles of comparable sizes. This argument, however, is not relevant in the present context of the new inflationary universe model.
[14]K. Maeda, K. Sato, M. Sasaki, and H. Kodama, Phys. Lett. **108B**, 98 (1982).
[15]W. Israel, Nuovo Cimento **44B**, 1 (1966); **48B**, 463(E) (1967).
[16]J. Ipser and P. Sikivie, Phys. Rev. D **30**, 712 (1984).
[17]V. A. Berezin, V. A. Kuzmin, and I. I. Tkachev, Phys. Lett. **120B**, 91 (1983).

[18]V. A. Berezin, V. A. Kuzmin, and I. I. Tkachev, *Quantum Gravity*, proceedings of the Third Seminar, Moscow, 1984, edited by M. A. Markov, V. A. Berezin, and V. P. Frolov (World Scientific, Singapore, 1985), p. 605.

[19]A. Aurilia, G. Denardo, F. Legovini, and E. Spallucci, Phys. Lett. **147B**, 258 (1984); Nucl. Phys. **B252**, 523 (1985).

[20]We follow the sign conventions of Ref. 21, in which the key definitions are given by $\Gamma^{\mu}_{\lambda\sigma}=\frac{1}{2}g^{\mu\nu}(\partial_{\lambda}g_{\nu\sigma}+\partial_{\sigma}g_{\nu\lambda}-\partial_{\nu}g_{\lambda\sigma})$, $V^{\mu}{}_{;\nu}=\partial_{\nu}V^{\mu}+\Gamma^{\mu}_{\nu\lambda}V^{\lambda}$, $V_{\mu;\nu}=\partial_{\nu}V_{\mu}-\Gamma^{\lambda}_{\mu\nu}V_{\lambda}$, $R^{\mu}{}_{\nu\alpha\beta}=\partial_{\alpha}\Gamma^{\mu}_{\nu\beta}-\partial_{\beta}\Gamma^{\mu}_{\nu\alpha}+\Gamma^{\mu}_{\sigma\alpha}\Gamma^{\sigma}_{\nu\beta}-\Gamma^{\mu}_{\sigma\beta}\Gamma^{\sigma}_{\nu\alpha}$, and $R_{\mu\nu}=R^{\alpha}{}_{\mu\alpha\nu}$.

[21]C. W. Misner, K. S. Thorne, and J. A. Wheeler, *Gravitation* (Freeman, San Francisco, 1973).

[22]M. D. Kruskal, Phys. Rev. **119**, 1743 (1960); G. Szekeres, Publ. Mat. Debrecen **7**, 285 (1960).

[23]G. W. Gibbons and S. W. Hawking, Phys. Rev. D **15**, 2738 (1977).

[24]We thank Sidney Coleman for suggesting this method of solution.

[25]The coordinate transformation can be represented most simply by introducing the lightlike coordinates $\zeta_{\pm}\equiv V\pm U$. The line element then has the form $ds^2=f(\zeta_+,\zeta_-)d\zeta_+d\zeta_-+r^2(\zeta_+,\zeta_-)d\Omega^2$, a form which is preserved by any transformation of the form $\zeta'_+=g(\zeta_+),\zeta'_-=h(\zeta_-)$. This transformation can be chosen so that each line in the de Sitter region corresponding to $\zeta_+=$const is assigned the value of ζ'_+ which is equal to the value of ζ_+ at the point where this line intersects the Schwarzschild region, and similarly for each line corresponding to $\zeta_-=$const. The values of $\zeta_{\pm}$ for lines which do not intersect the Schwarzschild region can be chosen arbitrarily.

[26]S. Coleman and F. De Luccia, Phys. Rev. D **21**, 3305 (1980). See also Sec. 6 of Ref. 13, which includes a discussion of a spacetime region which was omitted in the original reference.

[27]A. Vilenkin, Phys. Lett. **117B**, 25 (1982); Phys. Rev. D **27**, 2848 (1983); **30**, 509 (1984).

[28]J. B. Hartle and S. W. Hawking, Phys. Rev. D **28**, 2960 (1983); see also I. G. Moss and W. A. Wright, *ibid.* **29**, 1067 (1984); S. W. Hawking and J. C. Luttrell, Phys. Lett. **143B**, 83 (1984).

[29]A. D. Linde, Pis'ma Zh. Eksp. Teor. Fiz. **38**, 149 (1983) [JETP Lett. **38**, 176 (1983)]; Phys. Lett. **129B**, 177 (1983); A. B. Goncharov and A. D. Linde, *ibid.* **139B**, 27 (1984).

[30]E. Farhi and A. H. Guth, Phys. Lett. **183B**, 149 (1987).

[31]This question is academic, since the energies that are required are totally inaccessible. We found in Sec. V that the minimum mass necessary for what we called a monotonic trajectory is about 10^{28} GeV, and we presume that an energy of this order would be necessary to produce an inflationary universe by any laboratory mechanism.

[32]We thank Bill Press for helping us clarify the issues involved in this question.

[33]The quantum instability of Minkowski space has also been discussed by E. Gunzig and P. Nardone, Gen. Relativ. Gravit. **16**, 305 (1984), but they are writing about a different kind of instability.

[34]L. F. Abbott, Phys. Lett. **150B**, 427 (1985).

[35]G. 't Hooft, Nucl. Phys. **B256**, 727 (1985); in *Proceedings of the Symposium on Anomalies, Geometry, and Topology*, Argonne, Illinois, 1985, edited by W. A. Bardeen and A. R. White (World Scientific, Singapore, 1985), pp. 33–49.